Chapter 2

SYNTHESIS, CHARACTERIZATION, AND REACTIVITY OF ETHYNYL-TERMINATED Si(111) SURFACES

Plymale, N. T.; Kim, Y.-G.; Soriaga, M. P.; Brunschwig, B. S.; Lewis, N. S. Synthesis, Characterization, and Reactivity of Ethynyl- and Propynyl-Terminated Si(111) Surfaces. *J. Phys. Chem. C* **2015**, *119*, 19847–19862. DOI: 10.1021/acs.jpcc.5b05028

2.1 INTRODUCTION

The chemical structure at the surface of crystalline Si determines the susceptibility of the surface to oxidation or corrosion[1-3] and strongly influences electronic properties, such as the lifetimes of photogenerated charge carriers[4-5] and the positions of the semiconductor band edges.[6-7] Accordingly, chemical functionalization of the Si surface is a powerful tool for controlling the physical and chemical properties of interfaces between Si and other materials[8-10] and is important for numerous applications, such as improving the efficiency of Si-based photovoltaic and photoelectrochemical cells,[11-13] interfacing molecular electronics with Si-based circuitry,[14-16] improving semiconductor device electronics,[17-18] and interfacing molecular catalysts with electrode surfaces.[19-20]

Wet chemical methods offer a low-cost, scalable approach to functionalization of Si surfaces relative to methods that require vacuum or high temperatures. Covalent attachment of alkyl groups to the Si surface has been shown to impart beneficial properties, including resistance to oxidation[1-3] and low surface recombination velocity.[4, 21-22] However, correlation of the modified state of the surface with the changes to the chemical and physical properties that accompany the modification requires knowledge of the chemical structure of the functionalized surface. Of the alkyl-terminated surfaces studied, the CH_3–Si(111) surface has been characterized most extensively by methods including vibrational spectroscopy,[23-27] high-resolution X-ray photoelectron spectroscopy (XPS),[28-31] low-energy electron diffraction,[27-28] helium-atom scattering (HAS),[32-34] sum-frequency generation (SFG),[35] low-temperature scanning tunneling microscopy (STM),[36] and surface recombination velocity (S) measurements.[4] This extensive characterization of the CH_3–Si(111) surface has supported the conclusion that nearly full termination of the atop Si(111) sites by Si–C bonds can be achieved, resulting in exceptional surface ordering and stability. The $–CH_3$ group is unique among saturated hydrocarbons in this respect, whereas termination of Si(111) sites with ethyl ($–C_2H_5$) groups results in 60–90% termination in Si–C bonds with the remainder of the Si(111) atop sites terminated by Si–H.[7, 23-24, 37-38] Formation of Si–H at sites not terminated by Si–C leaves the surface susceptible to oxidation and concomitant formation of surface states.[29]

Despite their favorable properties, CH_3–Si(111) surfaces offer few opportunities for controlled secondary functionalization. Such opportunities have attracted considerable attention for use in solar cells,[39-40] transistors,[41] and molecular sensors.[42-43] Mixed monolayers have been developed for Si surfaces to impart functionality for facile secondary chemistry while maintaining high Si–C termination and low S.[21] For example, Heck coupling has been developed for mixed methyl/thienyl monolayers,[22] molecular proton-reduction catalysts have been assembled on mixed methyl/bipyridyl monolayers,[19] and growth of Al_2O_3 by atomic-layer deposition (ALD) has been seeded by mixed methyl/propionaldehyde surfaces.[17]

Covalent attachment to the Si surface of groups that are similar in size to methyl groups, but that contain versatile functional groups, offers an alternative approach to imparting opportunities for secondary functionalization to Si surfaces that maintain high Si–C termination and low *S*. Ethynyl (–CCH) groups have radial diameters and structures comparable to $-CH_3$ groups, making them geometrically suitable for nearly full termination of Si(111) atop sites with Si–CCH groups. Moreover, deprotonation of the HCC–Si(111) functional group should, in principle, allow facile chemical reactivity by a variety of synthetic routes and should change the surface functionalization chemistry from electrophilic attack chemistry, such as Cl–Si(111) reacting with RLi or RMgX, to nucleophilic attack chemistry performed by the acetylide-functionalized Si surface. Complete termination of Si(111) atop sites by Si–CCH groups would thus provide an organic scaffold for secondary functionalization of Si surfaces with molecular redox couples and catalysts, heterogeneous catalysts, metal films, ALD-grown protecting films, and conducting polymers, while preserving full termination of the Si atop sites by Si–C bonds.

The synthesis of HCC−Si(111) surfaces has been reported previously and extensively cited.[44-48] However, little structural characterization of the HCC–Si(111) surface has been reported, and notable inconsistencies exist between the reported syntheses and spectroscopic characterization of these surfaces. Further characterization of these surfaces is therefore needed to fully define the functionalization chemistry and to describe the properties of the modified Si(111) surfaces. We describe herein the synthesis of the HCC–Si(111) surfaces and provide extensive characterization of the modified surfaces by transmission infrared spectroscopy (TIRS), high-resolution electron energy-loss spectroscopy (HREELS), X-ray photoelectron spectroscopy (XPS), atomic-force microscopy (AFM), electrochemical scanning-tunneling microscopy (EC-STM), low-energy electron diffraction (LEED), and surface recombination velocity (*S*) measurements. We also describe an investigation of the reactivity of the terminal alkyne moiety in HCC–Si(111) surfaces. Furthermore, we have compared that reactivity with the reactivity of CH_3–Si(111) and propynyl-terminated Si(111) (CH_3CC–Si(111)) (see Chapter 3) surfaces. Additionally, we have compared the results of the surface analysis presented herein with previously reported data for ethynyl-terminated Si surfaces.

2.2 EXPERIMENTAL SECTION

2.2.1 Materials and Methods

Water (≥18.2 MΩ cm resistivity) was obtained from a Barnstead E-Pure system. Ammonium fluoride (NH_4F(aq), 40%, semiconductor grade, Transene Co., Inc., Danvers, MA) was purged with Ar(g) (99.999%, Air Liquide) for 1 h prior to use. Bromine (≥99.99% metal basis, Sigma-Aldrich) was purified by four freeze-pump-thaw cycles and dried over activated 3 Å molecular sieves (Sigma-Aldrich) prior to use. 4-fluorobenzyl chloride (99%, Sigma-Aldrich) was purified by four freeze-pump-thaw cycles and stored in a N_2(g)-purged glovebox prior to use. Dimethyl sulfoxide (DMSO, anhydrous, ≥99.9%, Sigma-Aldrich) and *N,N*-dimethylacetamide (DMA, anhydrous, 99.8%, Sigma-Aldrich) were dried over activated 3 Å molecular sieves prior to use. Sodium acetylide (NaCCH, ≥95%, 17.3% (w/w) in xylenes, Alfa Aesar) was filtered and washed with hexanes (anhydrous, mixture of isomers, ≥99%, Sigma-Aldrich) under an inert atmosphere. Dry NaCCH powder was stored in sealed glass containers under an inert atmosphere at 22 °C. All other chemicals were used as received.

Czochralski-grown n-Si wafers (Virginia Semiconductor, Fredericksburg, VA) used for the collection of XPS, AFM, EC-STM, LEED, and HREELS data were double-side polished, doped with phosphorus to a resistivity of 1 Ω cm, 381 ± 25 µm thick, and oriented to within 0.1° of the (111) crystal plane. Collection of TIRS data was performed using wafers with one of the following specifications: float-zone-grown n-Si wafers (Silicon Quest International, Santa Clara, CA), double-side polished, doped with phosphorus to a resistivity of 63–77 Ω cm, 435 ± 10 µm thick, and oriented to within 0.5° of the (111) crystal plane; or float-zone-grown Si wafers (Addison Engineering Inc., San Jose, CA), double-side polished, undoped with a resistivity of >20 kΩ cm, 500 ± 20 µm thick, and oriented to within 0.5° of the (111) crystal plane. Undoped, float-zone-grown Si wafers (FZWafers.com, Ridgefield Park, NJ) with a resistivity of 20–40 kΩ cm used for *S* measurements were double-side polished, 300 ± 25 µm thick, and oriented to within 0.5° of the (111) crystal plane. The wafer thickness was determined using calipers prior to performing *S* measurements.

Scheme 2.1 summarizes the methods used for the synthesis of CH_3–Si(111) and HCC–Si(111) surfaces.

Scheme 2.1. Synthesis of CH_3–Si(111) and HCC–Si(111) Surfaces

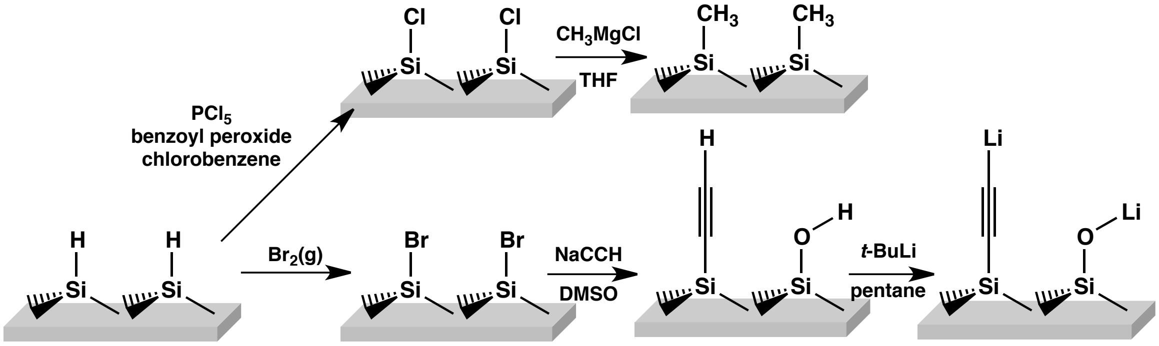

1. Preparation of Atomically Flat H–Si(111) Surfaces. Wafers were cut with a diamond-tipped scribe to the desired size and then rinsed sequentially with water, methanol (≥99.8%, EMD), acetone (≥99.5%, EMD), methanol, and water. Organic contaminants were removed and the surfaces were oxidized by immersing the wafers in a freshly prepared piranha solution (1:3 v/v of 30% H_2O_2(aq) (EMD): 18 M H_2SO_4 (EMD)) at 90–95 °C for 10–15 min. The wafers were rinsed with copious amounts of water and immersed in buffered HF(aq) (semiconductor grade, Transene Co., Inc.) for 18 s followed by another water rinse. Atomically flat H–Si(111) surfaces were prepared by immersing the wafers in an Ar(g)-purged solution of NH_4F(aq).[22, 49] Wafers with a miscut angle of 0.5° were etched for 5.5 min, while wafers with a miscut angle of 0.1° were etched for 9.0 min to obtain optimal terrace size. The solution was purged throughout the etching process and the wafers were agitated after each minute of etching to remove bubbles that formed on the surface. After etching, the wafers were rinsed with water and dried under a stream of Ar(*g*).

2. Preparation of Cl–Si(111) Surfaces. Cl–Si(111) surfaces were prepared for the synthesis of CH_3–Si(111) surfaces (see Chapter 1). Cl–Si(111) surfaces were prepared inside a $N_2(g)$-purged glovebox with <10 ppm $O_2(g)$. A saturated solution of PCl_5 (≥99.998% metal basis, Alfa Aesar) in chlorobenzene (anhydrous, ≥99.8%, Sigma-Aldrich) was preheated with an initiating amount (<1 mg mL^{-1}) of benzoyl peroxide (≥98%, Sigma-Aldrich) for 1–2 min. The H–Si(111) wafers were rinsed with chlorobenzene and then reacted in the PCl_5 solution at 90 ± 2 °C for 45 min.[22, 50] Upon completion of the reaction, the solution was drained and the wafers were rinsed with copious amounts of chlorobenzene, followed by tetrahydrofuran (THF, anhydrous, inhibitor-free, ≥99.9%, Sigma-Aldrich).

3. Preparation of of Br–Si(111) Surfaces. Br–Si(111) surfaces were prepared for the formation of HCC–Si(111) surfaces. Br–Si(111) surfaces were prepared by reaction under ambient light at 22 °C of H–Si(111) with $Br_2(g)$ in a drying chamber connected to a vacuum line as well as to a reservoir of $Br_2(l)$. Immediately after anisotropic etching, H–Si(111) samples were placed inside the drying chamber, which was then evacuated to <20 mTorr. The sample was sealed under vacuum and the $Br_2(l)$ reservoir was quickly opened and closed to allow a visible amount of $Br_2(g)$ into the evacuated drying chamber. The reaction was allowed to proceed for 10 s, after which the $Br_2(g)$ was removed by vacuum to a pressure of <20 mTorr.[7, 49] The sample was sealed under vacuum and transferred to a $N_2(g)$-purged glovebox.

4. Alkylation of Halogenated Si(111) Surfaces. CH_3–Si(111) surfaces were formed by the reaction of Cl–Si(111) surfaces with CH_3MgCl (1.0–3.0 M in THF, Sigma-

Aldrich or Acros Organics) at (45–60) ± 2 °C for 3–24 h.[22] HCC–Si(111) surfaces were formed by the reaction of Br–Si(111) surfaces with NaCCH in DMSO (allowed to saturate at 22 °C for 12–24 h) at 45 ± 2 °C for 4–8 h. The reaction of Br–Si(111) surfaces with NaCCH was performed in foil-covered test tubes to limit exposure of the NaCCH to ambient light. In several cases, HCC–Si(111) surfaces were also prepared using NaCCH in DMA (allowed to saturate at 22 °C for 12–24 h) at 45 ± 2 °C for 4–8 h. However, HCC–Si(111) surfaces prepared using DMA were not chemically well-defined, so HCC–Si(111) surfaces were prepared using DMSO unless otherwise stated. Upon completion of the reaction, CH_3–Si(111) samples were rinsed with and submerged in THF, removed from the glovebox, and sonicated for 10 min in each of THF, methanol, and water, respectively; HCC–Si(111) samples were rinsed with DMSO or DMA, then rinsed with and submerged in methanol (≥99.8%, anhydrous, Sigma-Aldrich), removed from the glovebox, sonicated for 10 min in methanol, and rinsed with water. Samples were dried under a stream of Ar(g) or N_2(g).

5. Deprotonation of HCC–Si(111) Surfaces and Subsequent Reactivity. Deprotonation of HCC–Si(111) surfaces was achieved by soaking the wafers in *tert*-butyllithium (*t*-BuLi, 1.7 M in pentane, Sigma-Aldrich) for 1 h at room temperature inside a N_2(g)-purged glovebox and subsequently rinsing with hexanes. Deprotonation was also performed for 1 h at room temperature using *n*-butyllithium (*n*-BuLi, 1.6 M in hexane, Sigma-Aldrich), lithium 2,2,6,6-tetramethylpiperidide (LiTMP, 1.0 M in THF, Sigma-Aldrich), lithium hexamethyldisilazide (LiHMDS, 1.0 M in hexane, Sigma-Aldrich) or lithium diisopropylamide (LDA, 1.0 M in THF/hexanes, Sigma-Aldrich) and yielded similar results to those reported herein with *t*-BuLi used as the deprotonating agent. The deprotonated wafers were then submerged for 1 h at room temperature in neat CD_3OD (99.6 atom % D, Sigma-Aldrich) to yield DCC–Si(111) surfaces or for 4 h at 50 ± 2 °C in neat 4-fluorobenzyl chloride to attach 4-fluorobenzyl groups to the surface. DCC–Si(111) surfaces were allowed to dry inside the glovebox and were sealed inside a centrifuge tube for transport to the IR spectrometer. Surfaces functionalized with 4-fluorobenzyl groups were rinsed with THF, submerged in THF, and removed from the glovebox. The wafers were then rinsed with water, dried under Ar(g), and transported to the XPS for analysis.

2.2.2 Instrumentation

1. Transmission Infrared Spectroscopy. TIRS data were collected using a Thermo Scientific Nicolet 6700 Fourier-transform infrared (FTIR) spectrometer equipped with an electronically temperature-controlled (ETC) EverGlo mid-IR source, a thermoelectric-cooled deuterated L-alanine doped triglycine sulfate (DLaTGS) detector, a KBr beam splitter, and a N_2(g) purge. A custom attachment allowed Si samples (1.3 × 3.2 cm) to be mounted such that the incident IR beam was either 74° or 30° with respect to the sample surface normal. At 74° (Brewster's angle for Si), IR modes parallel and perpendicular to the surface are observed, and at 30°, parallel modes remain visible, while perpendicular modes are greatly diminished in intensity.[23] Reported spectra are averages of 1500 consecutive scans collected at a resolution of 4 cm^{-1}. The baseline was flattened and peaks resulting from water absorption were subtracted in the reported spectra. Background SiO_x and H–Si(111) spectra were recorded separately for each sample prior to subsequent functionalization. Data were collected and processed using OMNIC software v. 9.2.41.

2. High-Resolution Electron Energy-Loss Spectroscopy. HREELS data were collected at pressures of $<5 \times 10^{-10}$ Torr using an LK Technologies ELS5000 model spectrometer equipped with a multichannel analyzer (MCA). Spectra were collected in the specular geometry for the instrument, with the electron impact and scattering angle both at 55° with respect to the sample surface plane. The monochromatic electron beam had an energy of 5.0 eV for CH_3–Si(111) surfaces and 2.8 eV for HCC–Si(111) surfaces. Prior to acquiring data, CH_3–Si(111) samples were annealed to 350 °C for 1 h in a separate vacuum chamber, while spectra of HCC–Si(111) samples were acquired without annealing. The y-axis value of each data point was averaged with the eight nearest-neighboring points to smooth the spectra.

3. Low-Energy Electron Diffraction. LEED patterns were collected at pressures $<5 \times 10^{-9}$ Torr using an LK Technologies RVL2000 instrument equipped with reverse-view optics, allowing images to be collected from behind the electron-gun assembly. The patterns were collected using a filament current of 3.05 A, a CAN voltage of 6.0 V, a screen voltage of 3.0 kV, and a retarding voltage of 100 V. The incident electron-beam energy was varied from 30–60 eV, and images exhibiting sharp patterns were obtained using a Canon EOS Rebel Tli camera with a 10 s exposure.

4. X-ray Photoelectron Spectroscopy and Thermal Stability Measurements. XPS data were collected at pressures $<5 \times 10^{-9}$ Torr using a Kratos AXIS Ultra spectrometer described previously and equipped with a monochromatic Al Kα X-ray source (1486.7 eV), a hybrid electrostatic and magnetic lens system, and a delay-line detector.[7, 49] Photoelectrons were collected at 90° with respect to the surface plane of the sample, with the lens aperture set to sample a 700 × 300 μm spot. The instrument was operated by Vision Manager software v. 2.2.10 revision 5. Survey and high-resolution scans were collected with analyzer pass energies of 80 eV and 10 eV, respectively. No signals from Cl, Br, Mg, Na, or Li impurities were detected on alkylated samples prepared as described. When HCC–Si(111) surfaces were prepared using DMA as the solvent, however, residual Br and N were often observed by XPS.

Thermal stability in vacuum was studied by collecting XP spectra as a function of annealing temperature. Samples were mounted on a resistive heating stage that consisted of a molybdenum puck heated with a tungsten wire. Stainless-steel clips affixed the sample to the molybdenum stage. The temperature was monitored by a type E thermocouple gauge affixed on the molybdenum stage immediately below the sample. Samples were heated to the desired temperature at a ramp rate of 10 °C min^{-1} and were held at the indicated temperature for 30 min. The samples were allowed to cool to 22–30 °C prior to collection of XPS data.

5. *Surface Recombination Velocity Measurements.* *S* measurements were performed by use of a contactless microwave conductivity decay apparatus described previously.[20-22] Electron-hole pairs were formed by a 20 ns, 905 nm laser pulse from an OSRAM diode laser with an ETX-10A-93 driver. For each laser pulse, the decay in reflected microwave intensity was monitored by a PIN diode connected to an

oscilloscope. All recorded decay curves were averages of 64 consecutive decays. Between measurements, samples were stored in air-filled centrifuge tubes in the dark.

6. Atomic-Force Microscopy. AFM images were collected using a Bruker Dimension Icon AFM operated by Nanoscope software v. 8.15. Images were collected in ScanAsyst mode using Bruker ScanAsyst-Air probes. The scanner z-range was set to 2 μm and a ScanAsyst noise threshold of 50–100 pm was used. Surface topography data were collected at a scan rate of 0.5–1.0 Hz for 1 μm^2 images. Data were processed using Nanoscope Analysis software v. 1.40.

7. Electrochemical Scanning-Tunneling Microscopy. In situ EC-STM studies were performed with a Nanoscope E (Digital Instruments, Santa Barbara, CA) equipped with a three-electrode potentiostat. The electrochemical cell was custom-crafted from Kel-F (Emco Industrial Plastics, Inc.) and fitted with a Pt counter and a Pt pseudoreference electrode calibrated against a Ag/AgCl reference cell. Tungsten tips were prepared by electrochemical etching of 0.25 mm diameter tungsten wire in 1.0 M KOH(aq) at a 15 V AC applied potential. All images were obtained under potential control in 0.1 M $HClO_4$(aq) with a high-resolution scanner in constant-current mode without post-scan processing.

2.2.3 Data Analysis

1. Fitting and Quantification of XPS Data. High-resolution XP spectra were analyzed using CasaXPS software v. 2.3.16. The peak positions for XP spectra were calibrated using the Si $2p_{3/2}$ peak, which was set to be centered at 99.68 eV.[28] For bulk

Si^0 and Si^{1+} doublets, the ratio of the peak area of the Si $2p_{1/2}$:$2p_{3/2}$ was set to 0.51 and the width of the two peaks was set equal.[28] Shirley backgrounds were used for all high-resolution data except when analyzing small amounts of SiO_x in the 102–104 eV range, for which a linear background was applied. C 1s and F 1s high-resolution spectra were fitted using the Voigt function GL(30), which consists of 70% Gaussian and 30% Lorentzian character. Si 2p photoemission signals for bulk Si^0 and Si^{1+} species were fitted using asymmetric Lorentzian line shapes convoluted with a Gaussian of the form LA(a, b, n), where a and b determine the asymmetry of the line shape and n specifies the Gaussian width of the function. LA(1.2, 1.4, 200) was found to fit consistently. Contributions from high-order SiO_x in the range of 102–104 eV were fit to a single peak using the GL(30) function.

The thickness (d_A) of the overlayer species A was estimated by XPS for HCC–Si(111) surfaces using the substrate-overlayer model[51-52]

$$\left(\frac{I_A}{I_{Si}}\right)\left(\frac{SF_{Si}}{SF_A}\right)\left(\frac{\rho_{Si}}{\rho_A}\right) = \left(\frac{1 - e^{\frac{-d_A}{\lambda_A \sin\theta}}}{e^{\frac{-d_A}{\lambda_{Si} \sin\theta}}}\right) \qquad (2.1)$$

where I_A is the area under the photoemission peak arising from the overlayer species A, I_{Si} is the area under the Si 2p photoemission signal, SF_{Si} is the instrument sensitivity factor for Si 2p (0.328), and SF_A is the instrument sensitivity factor for the overlayer species A, which is 0.278 for C 1s photoelectrons in hydrocarbon overlayers. For the hydrocarbon overlayers, I_A is the total area under the C 1s photoemission signal corresponding to all C atoms in the overlayer, which is the signal at 284.3 eV for CH_3–Si(111) surfaces and 284.5 eV for HCC–Si(111) surfaces. For Si–OH, I_A is the sum of the area under the Si 2p photoemission signal at 100.5 eV and 101.1 eV. For SiO_x, I_A is the area under the Si 2p photoemission signal appearing from 102–104 eV. The density of Si (ρ_{Si}) is 2.3 g cm^{-3}, and the density of the overlayer species A (ρ_A) is 3.0 g cm^{-3} for hydrocarbon overlayers.[30] HCC–Si(111) surfaces exhibited a fractional monolayer (ML) coverage of ~0.63 ML, so the assumed density of the overlayer was adjusted to model an overlayer with 63% of the density of a full monolayer (1.9 g cm^{-3}). When estimating the thickness of Si–OH or SiO_x overlayers, the quantity $(SF_{Si}/SF_A)(\rho_{Si}/\rho_A)$ reduces to a normalizing constant of 1.3 to account for the difference in Si 2p photoelectron signal intensity for Si–OH or SiO_x relative to bulk Si.[52] The attenuation length for the overlayer species (λ_A) has been estimated to be 3.6 nm for C 1s photoelectrons moving through hydrocarbon overlayers[53-54] or 3.4 nm for Si 2p photoelectrons moving through Si–OH or SiO_x overlayers.[53-54] The attenuation length for Si 2p photoelectrons (λ_{Si}) moving through hydrocarbon overlayers has been estimated to be 4.0 nm.[53-54] For Si–OH or SiO_x overlayers, the value of $\lambda_A = \lambda_{Si} = 3.4$ nm. The angle between the surface plane and the photoelectron ejection vector (θ) is 90°. The thickness of the overlayer species A was calculated using an iterative process.

The fractional monolayer coverage for the overlayer species A (Φ_A) was estimated by dividing the measured thickness, d_A, by the calculated thickness of 1 ML of overlayer species A, depicted in Scheme 2.2. The thickness of 1 ML of each hydrocarbon overlayer was estimated by summing the bond lengths for the species containing C, but excluding Si and H. For Si–OH overlayers, the thickness of 1 ML was estimated to be the distance from the bottom of the atop Si atom to the top of the O atom. The thickness of 1

ML of SiO_x was estimated to be 0.35 nm.[3, 52] Assuming uniform overlayers, the value of Φ_A represents the fraction of surface Si(111) sites that were modified with the overlayer species of interest.

Scheme 2.2. Monolayer Thickness of Surface-Bound $–CH_3$, –CCH, and –OH Groups

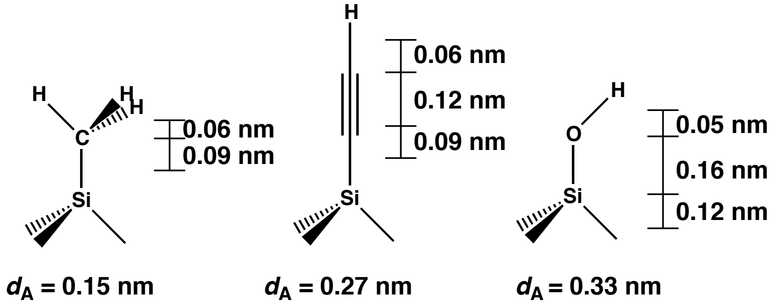

The fractional monolayer coverage for 4-fluorobenzyl-modified HCC–Si(111) and SiO_x surfaces was estimated using a three-layer model[55-56]

$$\left(\frac{I_\mathrm{A}}{I_\mathrm{Si}}\right)\left(\frac{SF_\mathrm{Si}}{SF_\mathrm{A}}\right)\left(\frac{\rho_\mathrm{Si}}{\rho_\mathrm{A}}\right)=\left(\frac{1-e^{\frac{-d_\mathrm{A}}{\lambda_\mathrm{A}\sin\theta}}}{e^{\frac{-(d_\mathrm{A}+d_\mathrm{B})}{\lambda_\mathrm{Si}\sin\theta}}}\right) \qquad (2.2)$$

where d_A is the thickness of the bound F atom and d_B is the thickness of the hydrocarbon layer between the Si crystal and the F atom. The value of SF_A for F 1s photoelectrons is 1.00 and the density of the overlayer was assumed to be the same as for HCC–Si(111) surfaces, 1.9 g cm^{-3}. For F 1s photoelectrons, the value of λ_A is 1.6 nm.[52] Scheme 2.3 shows the two proposed structures for 4-fluorobenzyl-modified HCC–Si(111) and SiO_x surfaces along with the calculated thickness for d_A and d_B. Since the ratio d_A/d_B is known from Scheme 2.3, eq 2.2 can be expressed in terms of d_A and solved using an iterative process. The measured thickness d_A was divided by the calculated thickness of 1 ML of F atoms, 0.13 nm, to give the fractional monolayer coverage of 4-fluorobenzyl groups.

Scheme 2.3. Monolayer Thickness of 4-Fluorobenzyl-Modified Surfaces

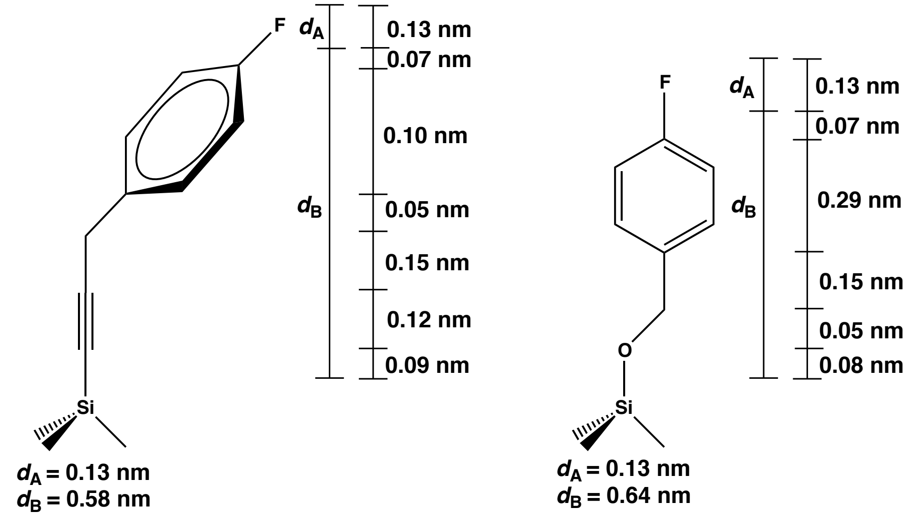

2. Calculation of Surface Recombination Velocity and Surface Trap-State Density. The minority-carrier lifetime (τ) was estimated by fitting the microwave conductivity decay versus time curve to an exponential decay, as described previously.[20-21] The calculated values of τ were converted to surface recombination velocities (S) for wafers of thickness d using[4-5, 21]

$$S = \frac{d}{2\tau} \qquad (2.3)$$

The surface recombination velocity was converted to an effective trap-state density, N_t, using[5, 22]

$$N_t = \frac{S}{\sigma v_{th}} \qquad (2.4)$$

where the trap-state capture cross section, σ, was 10^{-15} cm^2 and the thermal velocity of charge carriers, v_{th}, was 10^7 cm s^{-1}.[5] N_t can be used to estimate the absolute number of electrically active defects per surface Si(111) sites by use of the number density of atop Si sites for an unreconstructed Si(111) surface, $\Gamma_{Si(111)}$, which is 7.83×10^{14} atoms cm^{-2}.

Thus, a wafer with surface recombination velocity S has 1 electrically active defect for every $\Gamma_{\mathrm{Si(111)}}/N_t$ surface sites.

2.3 RESULTS

2.3.1 Transmission Infrared Spectroscopy

Figure 2.1 shows the TIRS data of HCC–Si(111) surfaces prepared in DMSO. The spectra exhibited two closely spaced signals at 3307 and 3296 cm^{-1}, corresponding to ethynyl ≡C–H stretching. The close spacing of these peaks resulted from asymmetric (3307 cm^{-1}) and symmetric (3296 cm^{-1}) stretching of the Si–C≡C–H unit as a whole. An additional sharp absorbance was observed at 2019 cm^{-1} and was indicative of C≡C stretching. These peaks were present at 74° incidence but absent at 30° incidence, which indicated that the stretching modes were oriented perpendicular to the sample surface. A weak but broad peak was observed from 950–1150 cm^{-1} at both angles of incidence and corresponded to transverse optical $(\mathrm{Si{-}O{-}Si})_{\mathrm{TO}}$ stretching.[23] The appearance of this peak at both angles of incidence suggested that the oxide was primarily subsurface. The spectra collected at 74° incidence also exhibited peaks at 3620, 1294, 920, and 836 cm^{-1}. The signal at 3620 cm^{-1} indicated O–H stretching,[57] while the signals at 920 and 836 cm^{-1} were characteristic of O–H bending and Si–O stretching, respectively.[58-60] The signal at 1294 cm^{-1} was tentatively assigned to O–H stretching coupled with O–H bending, following the analogous signal observed at 1080 cm^{-1} for methoxylated Si(111) surfaces that arises from O–C stretching rocking.[61] The observed signals suggested that a significant portion of the surface was hydroxylated and contained Si–OH functionality.

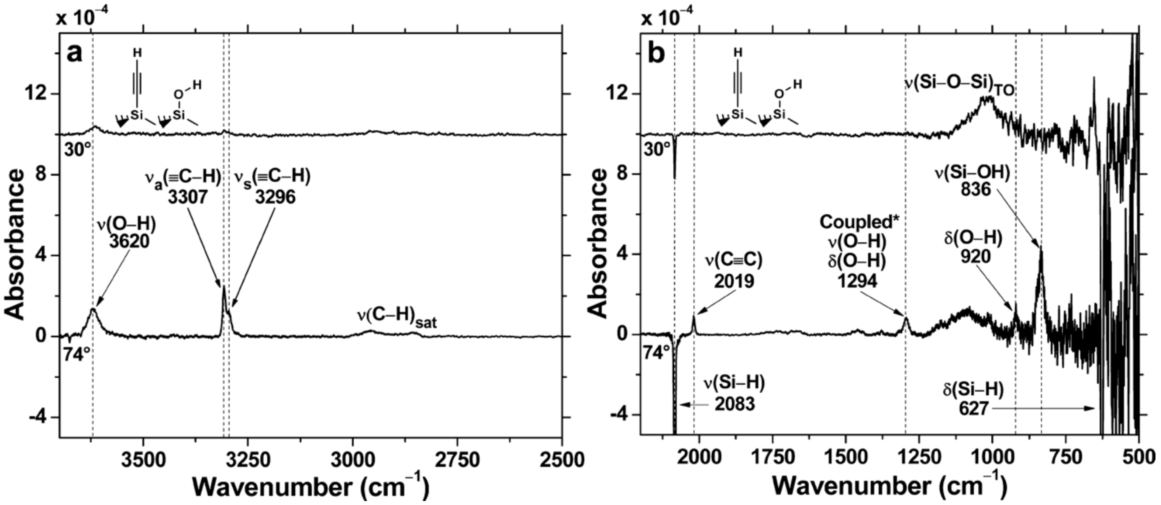

Figure 2.1. TIRS data for HCC–Si(111) surfaces prepared using DMSO, referenced to the H–Si(111) surface, and collected at incidence angles of 74° (bottom) and 30° (top) from the surface normal. Panel a shows the high-energy region, and panel b shows the low-energy region. The negative peaks in panel b resulted from the H–Si(111) background. The peak positions and assignments (∗ denotes tentative) are indicated in the figure. The subscript "sat" is used to denote C–H stretching signals arising from saturated hydrocarbons. The 30° spectrum is offset vertically for clarity.

TIRS data for HCC–Si(111) surfaces prepared using DMA as the solvent (Figure 2.2) exhibited peaks at 3307, 3292, and 2023 cm^{-1}, consistent with the ≡C–H and C≡C stretching signals observed for the surfaces prepared using DMSO. However, the modes at 3620, 1294, and 920 cm^{-1} were notably absent from surfaces prepared using DMA, and an absorbance at 828 cm^{-1} was lower in energy and intensity compared with the absorbance at 836 cm^{-1} for surfaces that were prepared using DMSO. Thus, surfaces prepared using DMA as the solvent did not exhibit the characteristic peaks for Si–OH sites on the surface. Additionally, surfaces prepared using DMA exhibited significantly stronger saturated hydrocarbon C–H stretching signals at 2947 and 2847 cm^{-1} in addition to several broad peaks between 1250 and 1700 cm^{-1}, which possibly arose from C–H bending and C–O or C=O stretching. Surfaces prepared using DMA also exhibited a significantly elevated intensity of the $(Si–O–Si)_{TO}$ mode centered at 1058 cm^{-1}.

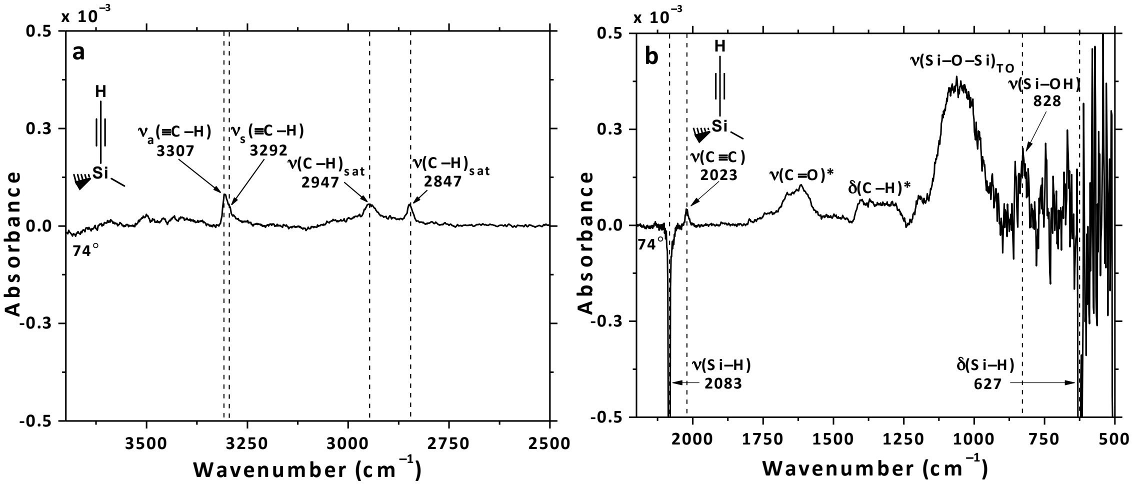

Figure 2.2. TIRS data for HCC–Si(111) surfaces prepared using DMA, referenced to the H–Si(111) surface and collected at 74° incidence. Panel a shows the high-energy region, and panel b shows the low-energy region. The negative peaks in panel b resulted from the H–Si(111) background. The subscript "sat" is used to denote C–H stretching signals arising from saturated hydrocarbons. The peak positions and assignments (∗ denotes tentative) are indicated in the figure.

Figure 2.3 shows the absence of detectable Si−H stretching for CH_3–Si(111) and HCC−Si(111) surfaces.

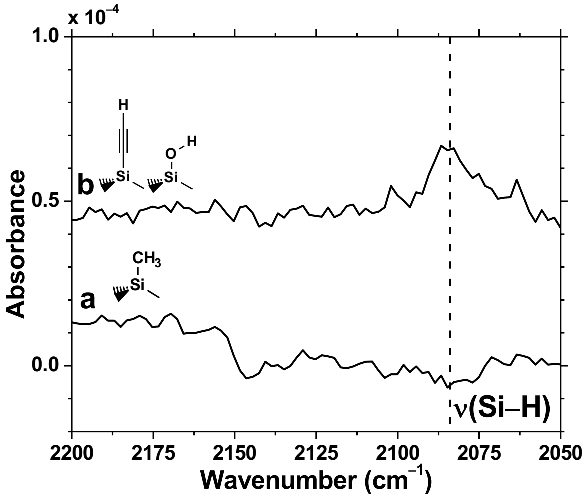

Figure 2.3. TIRS data for (a) CH_3–Si(111) and (b) HCC–Si(111) surfaces referenced to the SiO_x surface. The position of the Si–H stretching peak is indicated by the dotted line.

2.3.2 High-Resolution Electron Energy-Loss Spectroscopy

HREELS data were obtained for HCC–Si(111) surfaces to detect vibrational signals that could not be readily observed by TIRS. The HREELS data for HCC–Si(111) surfaces (Figure 2.4) showed signals centered at 2032 and 3307 cm^{-1}, corresponding to C≡C stretching and ethynyl ≡C–H stretching motions, respectively. A peak centered at 648 cm^{-1} is assignable to Si–C stretching, indicating that the ethynyl units had been covalently attached to the Si(111) surface. The presence of a peak at 2954 cm^{-1} arose from adventitious hydrocarbon species adsorbed to the sample surface, and a signal centered at 1072 cm^{-1} corresponded to the $(Si–O–Si)_{TO}$ mode observed by TIRS. A strong signal centered at 842 cm^{-1} resulted from surface Si–O stretching convoluted with

O–H bending derived from Si–OH surface sites. This assignment is supported by the presence of a peak centered at 3625 cm^{-1}, corresponding to O–H stretching. Thus, the presence of surface Si–CCH and Si–OH groups was confirmed by the HREELS data.

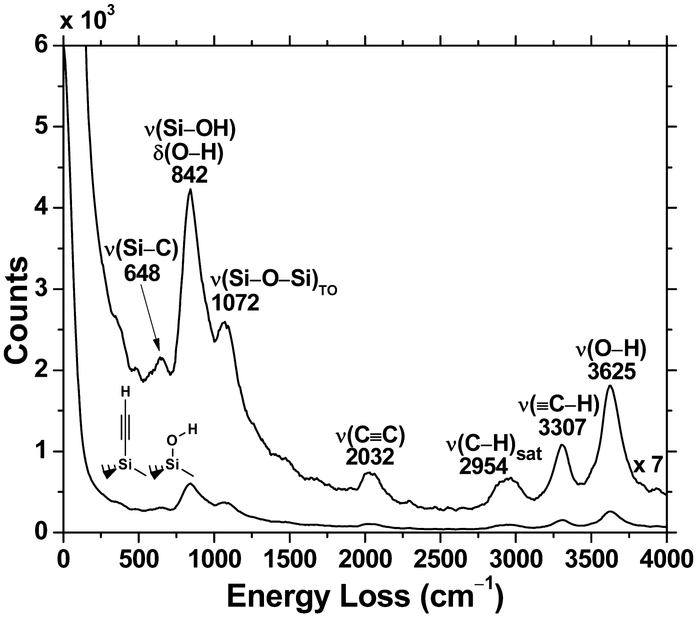

Figure 2.4. HREELS data for HCC–Si(111) surfaces. Data were collected in the specular geometry using an incident beam energy of 2.8 eV, and the fwhm of the elastic peak was 17.3 meV. The subscript "sat" is used to denote C–H stretching signals arising from saturated hydrocarbons. The raw spectrum (bottom) is shown with the magnified spectrum (top) superimposed for clarity. The peak positions and assignments are indicated in the figure.

The vibrational spectroscopy data for HCC–Si(111) surfaces is summarized in Table 2.1.

Table 2.1. Summary of the Positions and Assigned Modes for the Vibrational Signatures Observed for the HCC–Si(111) Surface

TIRS Frequency (cm^{-1})	**HREELS Frequency (cm^{-1})**[a]	**Assigned Mode**[b]	**Orientation to Surface**[c]
3620	3625	ν(O–H)	
3307	3307	ν_a(≡C–H)	⊥
3296	3307	ν_s(≡C–H)	⊥
weak	2954	ν(C–H)$_{sat}$	
2019	2032	ν(C≡C)	⊥
1294	1072	ν(O–H) and δ(O–H)∗	⊥
~1050	1072	ν(Si–O–Si)$_{TO}$	not ⊥
920	842	δ(O–H)	⊥
836	842	ν(Si–OH)	⊥
–	648	ν(Si–C)	

[a] In some cases, HREELS signals do not resolve multiple vibrational modes that are observed by TIRS. The HREELS signal with the closest energy to the resolved TIRS signal is paired in the table. [b] The symbols ν and δ signify stretching and bending motions, respectively, with subscripts a and s indicating whether the mode is asymmetric or symmetric, respectively. The subscript "TO" indicates a transverse optical Si–O–Si motion. The subscript "sat" indicates a C–H stretching signal arising from unidentified saturated hydrocarbons. The subscript "CCH" indicates C≡C stretching peaks arising from –CCH groups. The assignments marked with ∗ are tentative. [c] The orientation of the vibrational mode with respect to the plane of the sample surface determined by TIRS is given.

2.3.3 X-ray Photoelectron Spectroscopy.

XPS data were collected to provide quantitative information about the species present on HCC–Si(111) surfaces. Survey spectra showed only signals ascribable to Si, C and O, and high-resolution spectra were acquired for the C 1s and Si 2p core levels. Figure 2.5 shows the C 1s high-resolution XP spectrum for HCC–Si(111) surfaces. The C 1s spectrum showed a prominent photoemission signal at 284.5 eV in addition to two signals of lower intensity centered at 285.4 and 287.1 eV. The signals at 285.4 and 287.1 eV exhibited considerable variation in intensity and fwhm between samples and fell within the typical binding energy range for adventitious C on alkyl-terminated Si surfaces.[28] The signals arising from adventitious C species exhibited a broad fwhm relative to the signal from the −CCH group at 284.5 eV. The adventitious species exhibited an undefined chemical structure, and thus multiple C species contributed to the

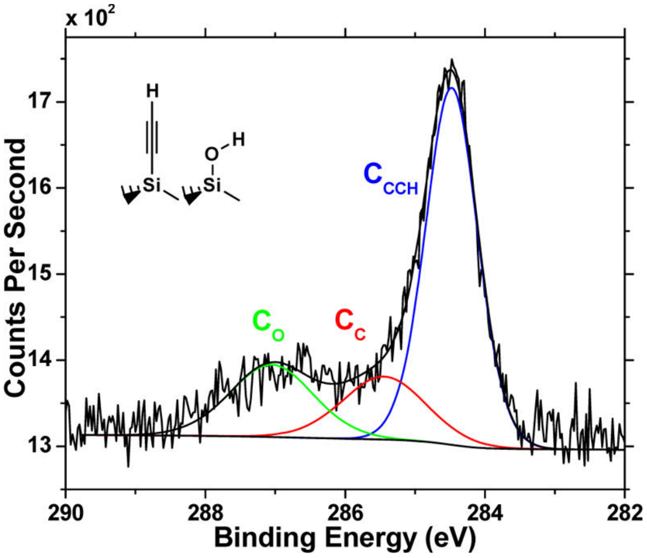

Figure 2.5. High-resolution XP spectrum of the C 1s region for HCC–Si(111) surfaces. The low binding energy C photoemission signal at 284.5 eV (blue, C_{CCH}) arises from both C atoms in the bound −CCH group. The peaks at 285.4 (red, C_C) and 287.1 eV (green, C_O) arise from adventitious C bound to C and C bound to O, respectively.

observed signals and led to broadening. The observed photoemission signal at 284.5 eV was centered at slightly higher binding energy than the photoemission signal ascribed to C bound to Si for CH_3–Si(111) surfaces.[21, 28] The fwhm of this signal was larger than was typically observed for the C bound to Si signal on CH_3–Si(111) surfaces at 284.3 eV, suggesting multiple contributions to the peak. Additionally, the absence of two fully resolved signals of comparable intensity suggests that the signal centered at 284.5 eV derives from two closely spaced photoemission signals with contributions from both C atoms in the –C≡CH group (C_{CCH}).

Figure 2.6 shows the high-resolution Si 2p spectrum for HCC–Si(111) surfaces. The spectra exhibited a shoulder on the high binding-energy side of the bulk Si $2p_{1/2}$ peak. This shoulder was fit to two peaks centered at 100.5 and 101.1 eV and was ascribed to

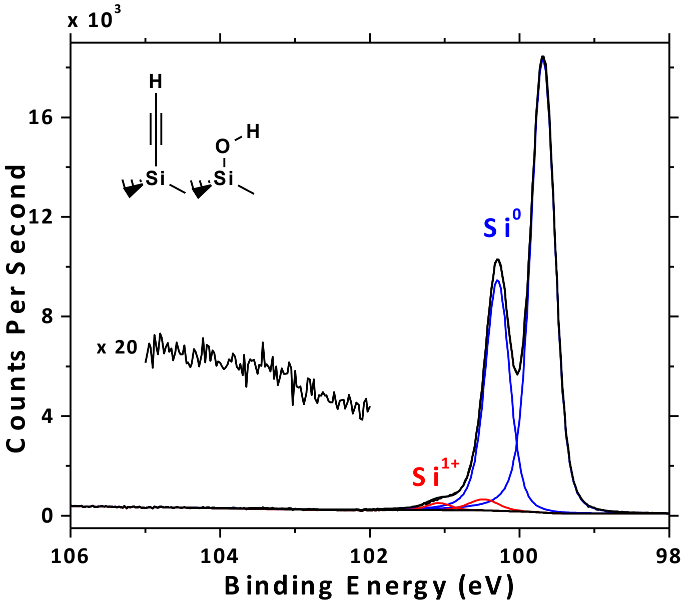

Figure 2.6. High-resolution XP spectrum of the Si 2p region for HCC–Si(111) surfaces. Contributions from the bulk Si (blue, Si^0) and Si^{1+} (red) species are indicated. The region from 102–105 eV in the Si 2p spectrum is magnified to show the absence of detectable high-order SiO_x.

Si–OH groups, in which the surficial Si is bound to a single O atom, consistent with results observed in the vibrational spectra. Some HCC–Si(111) samples showed the presence of a small, broad signal in the range of 102–104 eV, which was ascribed to SiO_x.

The fractional monolayer coverage for HCC–Si(111) surfaces was estimated by XPS, by use of eq 2.1,[51-52] to yield $\Phi_{Si–CCH} = 0.63 \pm 0.08$ ML. Only the area under the C 1s photoemission signal at 284.5 eV was used in the quantification of $\Phi_{Si–CCH}$ because it arises directly from the –CCH group. Vibrational spectroscopic signatures also indicated the presence of Si–OH groups, and XPS was also used to estimate the fractional ML coverage of Si–OH on HCC–Si(111) surfaces by use of eq 2.1[51-52] to yield $\Phi_{Si–OH} = 0.35 \pm 0.03$ ML. In addition to Si–OH, high-order oxide signals, between 102 and 104 eV, were observed in limited quantities in the Si 2p spectrum on some HCC–Si(111) surfaces with a fractional ML coverage estimated by eq 2.1[51-52] of $\Phi_{SiO_x} = 0.03 \pm 0.02$ ML. The content of high-order SiO_x was near the detection limit for the instrument for most samples, and several samples showed the absence of detectable high-order SiO_x.

The thermal stability of HCC–Si(111) surfaces was investigated in vacuum. Figure 2.7 presents the behavior of HCC–Si(111) surfaces as a function of annealing temperature. Minimal changes to the C 1s and Si 2p high-resolution spectra were observed for HCC–Si(111) surfaces upon annealing to 200 °C. However, heating to 300 °C produced significant broadening of the strongest photoemission signal in the C 1s spectrum, and a shoulder appeared at ~285.1 eV. The C 1s signal further broadened upon heating to 400 and 500 °C, respectively, which suggested that, at elevated temperature, the ethynyl group reacted with adventitious carbon species on the sample and in the

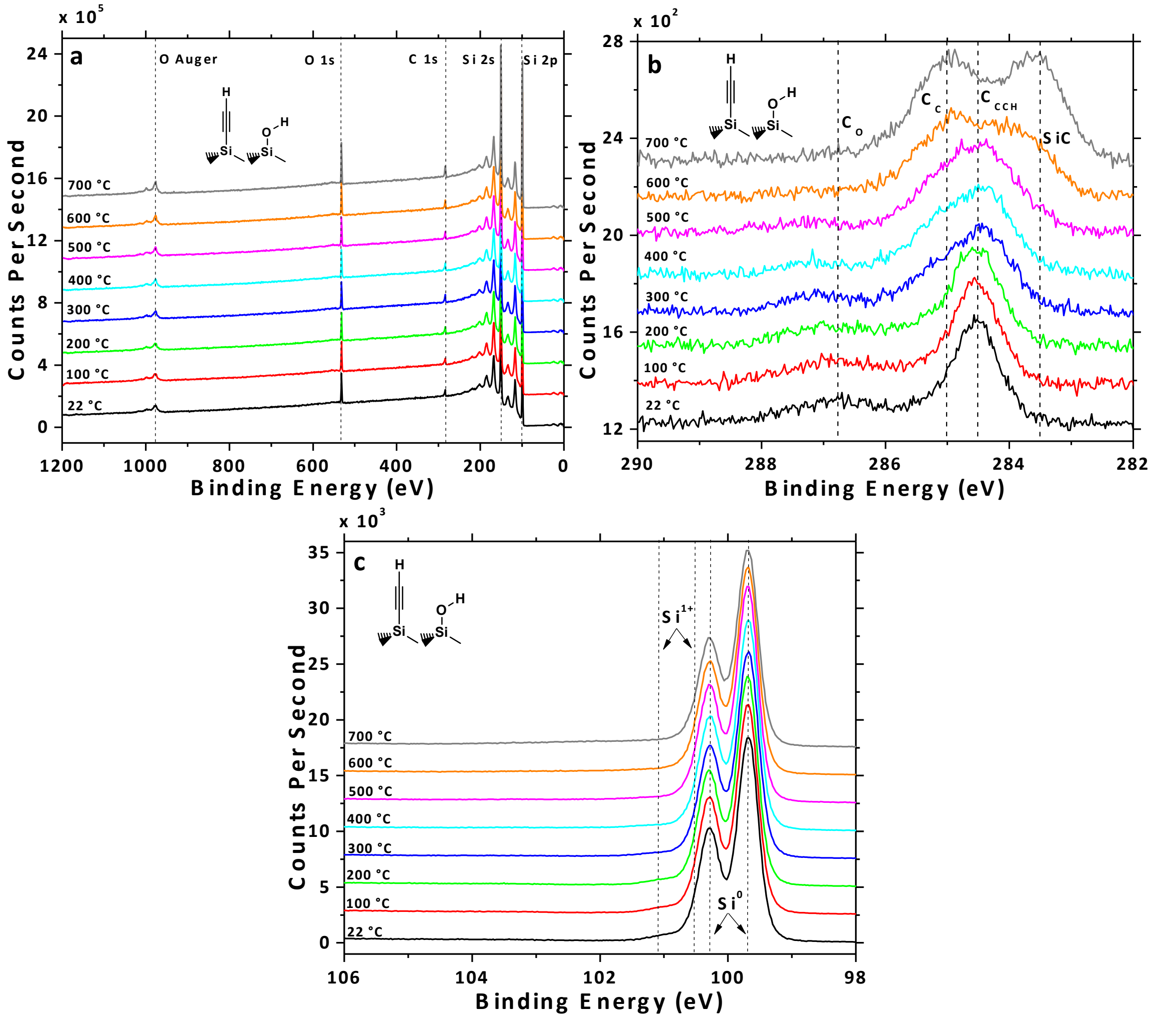

Figure 2.7. Thermal stability in vacuum of HCC–Si(111) surfaces. The annealing temperature is indicated above each spectrum, and the spectra are offset vertically for clarity. The survey spectra (a) showed the presence of only the Si 2p, Si 2s, C 1s, and O 1s core-level peaks along with the O Auger signal and Si plasmon-loss features. The high-resolution C 1s spectra (b) exhibited the peaks arising from C in the ethynyl group (C_{CCH}) and adventitious C (C_C and C_O). Minimal change in the C 1s spectra was observed upon annealing to 200 °C. Broadening was observed as the C 1s peak at ~285.1 eV (C_C) greatly increased in intensity upon heating to 300–500 °C. Heating to 600–700 °C resulted in the appearance of a new C 1s peak at ~283.5 eV (SiC). Si 2p spectra (c) showed gradual smoothing of the shoulder indicated as Si^{1+} with increased annealing temperature, indicating the loss of surficial Si–OH and formation of Si–O–Si.

vacuum chamber. Heating from 300 to 500 °C reduced the intensity of the signal at 284.5 eV, which indicated that the coverage of the Si(111) surface with chemically defined ethynyl groups decreased upon heating to this temperature range. Table 2.2 provides the estimated fractional monolayer coverage of the Si(111) surface with chemically defined –CCH groups as a function of annealing temperature. Heating to 600 and 700 °C, respectively, resulted in an increase in intensity and broadening of the overall C 1s signal. A signal at ~283.5 eV, which has been ascribed to silicon carbide (SiC),[31, 62-63] was observed after annealing to 600 °C and became more prominent after heating the sample to 700 °C. An increase in overall intensity of the C 1s photoemission signal after annealing to 700 °C indicated that additional C species were formed on the surface, though their chemical structure was not readily determined by the XPS measurements performed. The shoulder in the Si 2p photoemission signal on the high binding-energy side of the Si $2p_{1/2}$ peak became less prominent upon heating past 300 °C, suggesting the removal of surficial Si–OH groups. The survey spectra showed no reduction in O 1s peak intensity as a function of annealing temperature, so the detected O likely inserted between the Si backbonds to produce Si–O–Si. Additionally, a small reduction in the bulk Si 2p

Table 2.2. Estimated Fractional ML Coverage, Φ, of a HCC–Si(111) Surface as a Function of Annealing Temperature

Annealing Temperature (°C)	$\Phi_{\mathrm{Si-CCH}}{}^{a}$
22	0.62
100	0.60
200	0.53
300	0.34
400	0.28
500	0.10

[a] The values of Φ were determined using eq (2.1).[51-52] The appearance of SiC on HCC–Si(111) surfaces upon annealing to 600 °C precluded accurate determination of Φ beyond 500 °C.

signal intensity was observed after heating to 600 and 700 °C, respectively, as a result of the increase in C species on the surface.

2.3.4 Atomic-Force Microscopy, Electrochemical Scanning-Tunneling Microscopy, and Low-Energy Electron Diffraction

Figure 2.8 presents a representative topographical AFM image of an HCC–Si(111) surface. The HCC–Si(111) surface exhibited broad atomic terraces with step edges ~0.3 nm in height, consistent with terraces observed on reconstructed Si(111) surfaces in vacuum.[64] Generally, the surfaces exhibited a low density of particulates adsorbed to the surface, and the density of etch pits observed by AFM was low. The observation of atomic terraces after alkylation was consistent with the grafting of an overlayer with uniform thickness onto the surface of the Si(111) substrate.

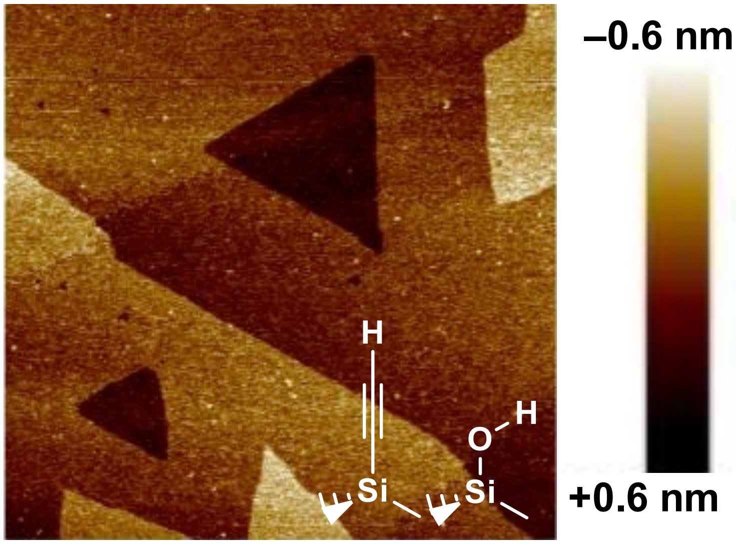

Figure 2.8. Topographical AFM image of the HCC–Si(111) surface. The image is 1 μm × 1 μm with a z-scale of 1.2 nm (–0.6 to +0.6 nm).

Figure 2.9 shows a representative EC-STM image of the HCC–Si(111) surface. The HCC–Si(111) surface showed localized areas where species of similar height were observed (representative areas indicated by white circles), consistent with the proposed mixed composition of HCC–Si(111) surfaces, in which a fraction of the surface sites are terminated by Si–OH. The distance between the centers of the areas with similar height was 0.38 nm, which is the same as the distance between Si(111) atop sites.[36] The majority of the HCC–Si(111) surface did not exhibit ordering on an atomic scale as observed by room temperature EC-STM.

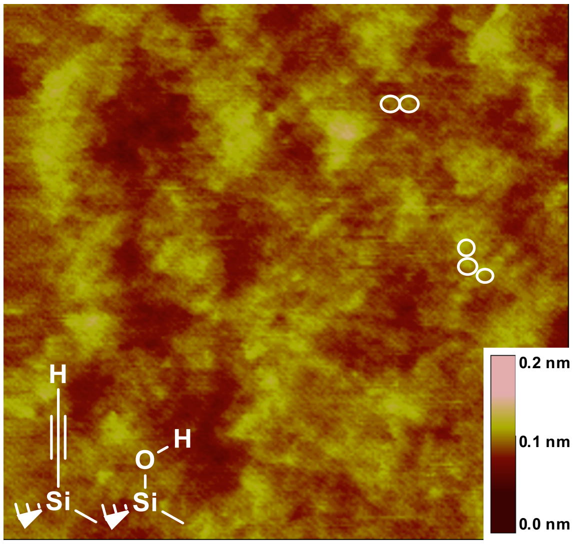

Figure 2.9. EC-STM image of the HCC–Si(111) surface (10 nm ×10 nm) collected at –0.4 V versus Ag/AgCl with a bias voltage of –300 mV and tunneling current of 5 nA. The z-scale is indicated in the figure. The white circles in the figure highlight areas where species of similar height were observed. The distance between the centers of the white circles was 0.38 nm, the same as the distance between Si(111) atop sites. Image courtesy of Y.-G. Kim and M. P. Soriaga.

LEED patterns were collected for HCC–Si(111) surfaces (Figure 2.10) to qualitatively determine the ordering of the top surface layers of the substrate. LEED patterns that exhibit 3-fold symmetry, with diffraction spots forming a hexagon, are indicative of a (1 × 1) surface unit cell. Generally, LEED has limited sensitivity on the monolayer scale, and disordered Si surfaces that exhibit high crystallinity of the Si immediately below the surface will still display clear diffraction spots. The qualitative intensity of the background relative to the diffraction spots can provide some degree of information about the ordering of the surface layer. HCC−Si(111) exhibited similar 3-fold symmetry with the presence of a hexagonal diffraction pattern appearing at 40 eV beam energy. The background appeared slightly more intense than for CH_3–Si(111) control samples, suggesting a lower level of ordering at the sample surface than for CH_3–Si(111). This behavior was consistent with the observed mixed composition of HCC–Si(111) surfaces, which showed vibrational signatures of Si–CCH and Si–OH groups.

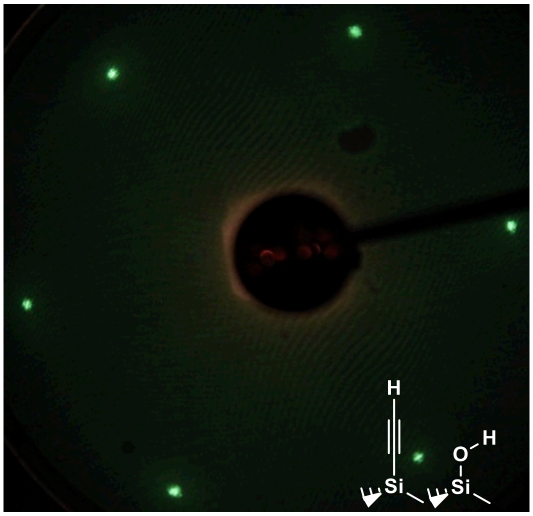

Figure 2.10. Representative LEED pattern for the HCC–Si(111) surface collected at 40 eV incident beam energy.

The HCC–Si(111) and CH_3–Si(111) surfaces exhibited comparably bright and sharp diffraction spots, and the only evidence of lower surface ordering for H–Si(111) samples was in the intensity of the background.

2.3.5 Surface Recombination Velocity Measurements

Figure 2.11 shows the behavior of *S* determined by use of eq 2.3[4] for CH_3–Si(111) and HCC–Si(111) surfaces as a function of time in air. Immediately after preparation and cleaning, CH_3–Si(111) and HCC−Si(111) surfaces exhibited *S* values of $(4 \pm 2) \times 10^1$ and $(2.5 \pm 0.3) \times 10^3$ cm s^{-1}, respectively. After being exposed to air for 24 h, the *S* value for CH_3–Si(111) surfaces decreased to $(1.5 \pm 0.5) \times 10^1$ cm s^{-1}, while HCC–Si(111) surfaces exhibited an increase in *S* to $(3.30 \pm 0.09) \times 10^3$ cm s^{-1}. Over extended exposure to air, *S* for HCC–Si(111) surfaces remained relatively constant at $(3.5 \pm 0.1) \times 10^3$ cm s^{-1}.

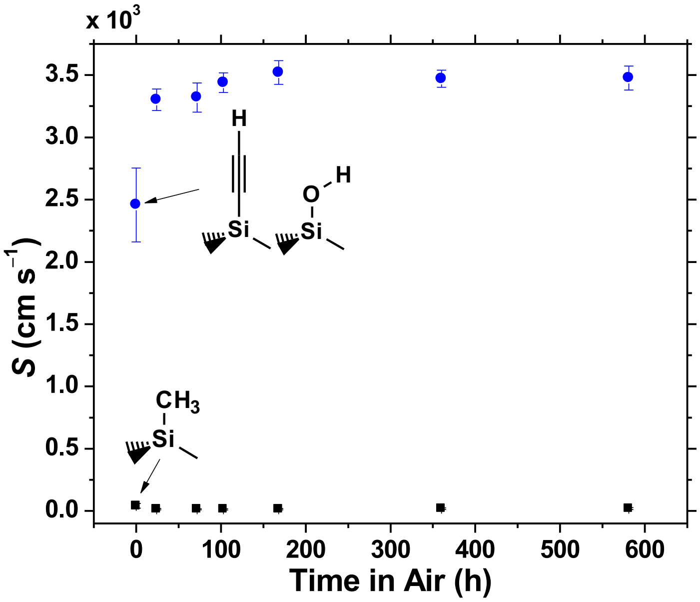

Figure 2.11. *S* measured as a function of exposure to air for CH_3–Si(111) (black squares) and HCC−Si(111) (blue circles) surfaces. The error bars represent 1 standard deviation about the mean.

The effective trap-state density, N_t, was calculated for CH_3–Si(111) and HCC–Si(111) surfaces by use of eq 2.4.[5] Immediately after preparation, CH_3–Si(111) and HCC–Si(111) surfaces were found to have trap-state densities of 4×10^9 and 3×10^{11} cm^{-2}, which is equivalent to 1 trap for every 2×10^5 and 3×10^3 surface sites, respectively. After 581 h of exposure to air, the trap-state densities of CH_3–Si(111) and HCC–Si(111) surfaces had adjusted to yield 2×10^9 and 3×10^{11} cm^{-2}, or 1 trap for every 4×10^5 and 2×10^3 surface sites, respectively. The estimated trap-state density for the studied surfaces was below the detection limit for most spectroscopies, hindering the identification of the chemical structures that form the surface trap states.

2.3.6 Reactivity of HCC–Si(111) Surfaces

The reactivity of the terminal alkyne moiety on HCC–Si(111) surfaces was explored by deprotonating the ethynyl group with a strong base. HCC–Si(111) surfaces were soaked in a *t*-BuLi solution to generate putative surface-bound Si–C≡C–Li groups. Such putative deprotonated surfaces were then soaked in CD_3OD to yield DCC–Si(111) surfaces. Figure 2.12 presents TIRS data for HCC–Si(111) surfaces before and after treatment with *t*-BuLi followed by CD_3OD. This treatment resulted in a reduction in the intensity of the ethynyl ≡C–H stretching (3307 and 3296 cm^{-1}) and C≡C stretching (2019 cm^{-1}) signals as well as in the appearance of new absorption peaks at 2574, 2559, and 1897 cm^{-1}. Figure 2.13 shows that the peaks were absent for samples collected at 30° incidence angle, indicating that the groups were oriented perpendicular to the surface. Similar results were obtained using other strong bases, such as *n*-BuLi, LiTMP, LiHMDS, and LDA, as shown in Figure 2.14, indicating that the surface-bound organolithium

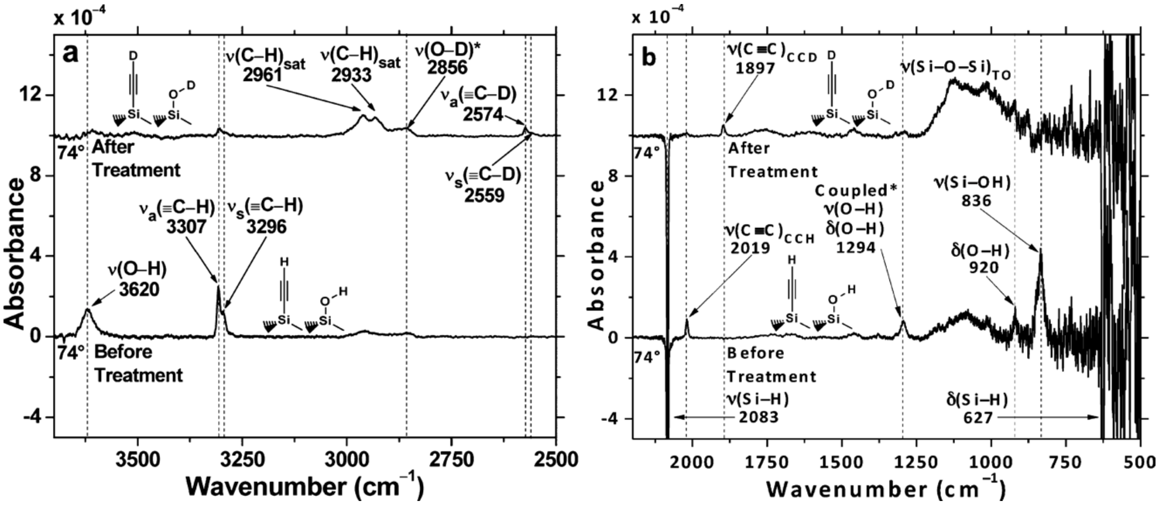

Figure 2.12. TIRS data for HCC–Si(111) surfaces referenced to the H–Si(111) surface before (bottom) and after (top) treatment with *t*-BuLi followed by CD_3OD. Panel a shows the high-energy region, and panel b shows the low-energy region. The peak positions and assignments (∗ denotes tentative) are indicated in the figure. The subscript "sat" is used to denote C–H stretching signals arising from saturated hydrocarbons and the subscripts CCH and CCD indicate vibrational modes arising from HCC–Si(111) and DCC–Si(111) moieties, respectively. The spectrum shown after treatment was offset vertically for clarity.

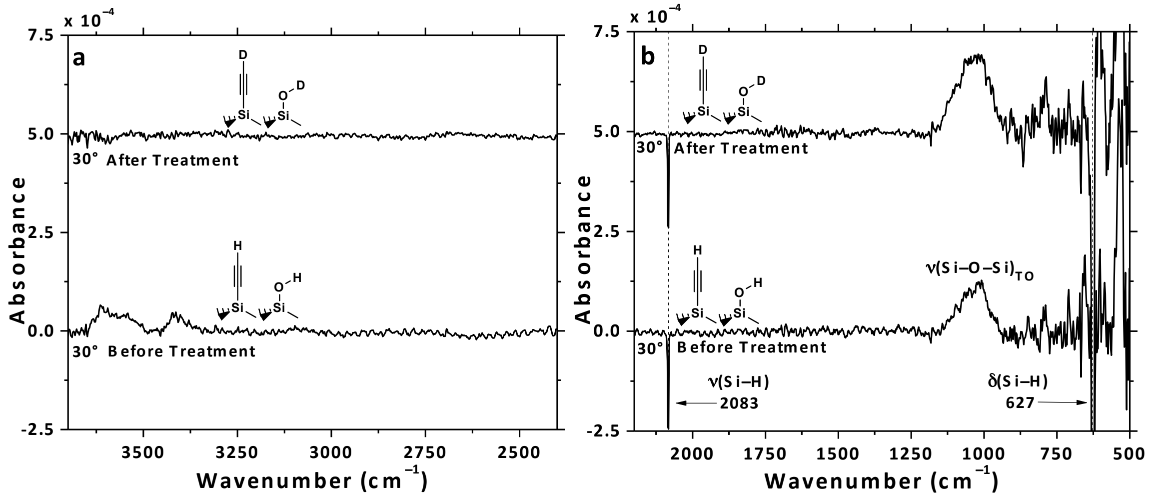

Figure 2.13. TIRS data for HCC–Si(111) surfaces referenced to the H–Si(111) surface collected at 30° incidence angle before (bottom) and after (top) treatment with *t*-BuLi followed by CD_3OD. Panel (a) shows the high-energy region, and panel (b) shows the low-energy region. The negative peaks in panel (b) resulted from the H–Si(111) background. The absence of any signals attributable to –CCD groups after treatment indicates that the modes observed at 74° are perpendicular to the surface. The spectrum collected after treatment is offset vertically for clarity.

species can be generated by reaction routes that are analogous to those displayed by small-molecule terminal alkynes. The shape and spacing of the peaks at 2574 and 2559 cm^{-1} were similar to the signals at 3307 and 3296 cm^{-1}, suggesting that these new peaks arose from ≡C–D asymmetric and symmetric stretching, respectively. The new signal at 1897 cm^{-1} was symmetric and positioned at slightly lower energy than the original C≡C stretching signal at 2019 cm^{-1}. The signal at 1897 cm^{-1} arose from C≡C stretching and was shifted to lower energy relative to the C≡C stretching signal for the HCC–Si(111) surface by introduction of the D atom to the ethynyl group. Integration of the area under

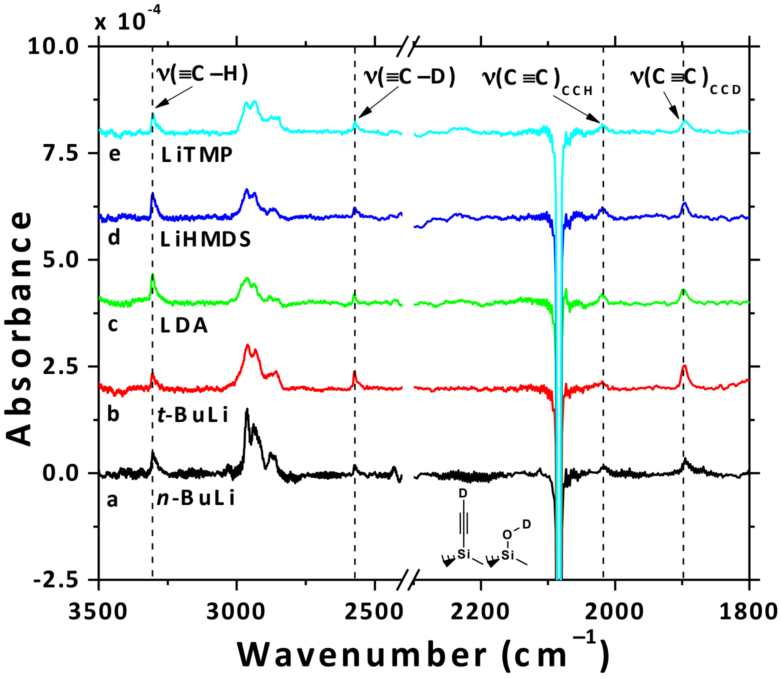

Figure 2.14. TIRS data collected at 74° incidence angle for HCC–Si(111) surfaces after treatment with (a) *n*-BuLi, (b) *t*-BuLi, (c) LDA, (d), LiHMDS, or (e) LiTMP followed by reaction with CD_3OD. The characteristic peaks corresponding to the –CCH and –CCD surface species are indicated by the dotted lines. The negative peak at 2083 cm^{-1} resulted from the H–Si(111) background. Spectra collected for all bases yielded comparable peaks ascribable to the surface –CCD species. The spectra were offset vertically for clarity.

the ethynyl ≡C–H stretching peaks at 3307 and 3296 cm^{-1} and under the C≡C stretching peak at 2019 cm^{-1} in the TIR spectra before and after deuteration showed that the peak area was reduced to roughly 22% of the original area. These data suggested that an estimated 78% of surface-bound ethynyl groups had been converted to Si–C≡C–D groups by this process.

Treatment of HCC–Si(111) surfaces with *t*-BuLi also deprotonated the surface-bound –OH groups, as evidenced by the disappearance of the peak at 3620 cm^{-1} (Figure 2.12). Several new peaks appeared at 2961, 2933, and 2856 cm^{-1} in the typical C–H stretching region for adventitious C species, but also resulted from O–D stretching in Si–OD groups. Figure 2.15 shows that this treatment also produced a peak at 2075 cm^{-1} observed in spectra that were referenced to the SiO$_x$ surface, and this signal can be

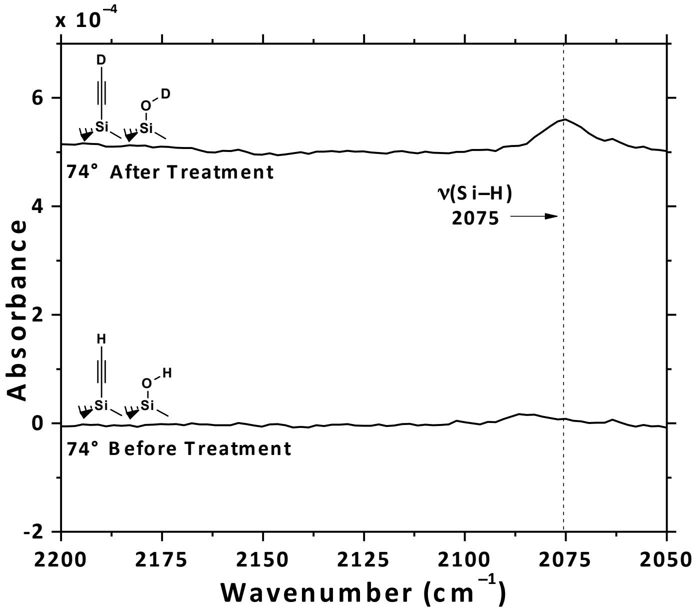

Figure 2.15. TIRS data collected at 74° incidence angle for HCC–Si(111) surfaces referenced to the SiO$_x$ surface before (bottom) and after (top) treatment with *t*-BuLi followed by CD$_3$OD. The center of the Si–H stretching peak is indicated by the dotted line, and the broad peak in the top spectrum at 2075 cm^{-1} is ascribed to Si–H stretching.

ascribed to Si–H stretching. The total area under the Si–H stretching signal was ~8% of the area of the signal on the fully terminated H−Si(111) surface. The vibrational data for the deprotonated DCC–Si(111) surface is summarized in Table 2.3.

Table 2.3. Summary of the Positions and Assigned Modes for the Vibrational Signatures Observed for the DCC–Si(111) Surface

TIRS Frequency (cm^{-1})	**Assigned Mode**[a]	**Orientation to Surface**[c]
3307	ν_a(≡C–H)	⊥
3296	ν_s(≡C–H)	⊥
2961	ν(C–H)$_{sat}$	
2933	ν(C–H)$_{sat}$	
2856	ν(O–D)∗	
2574	ν_a(≡C–D)	⊥
2559	ν_s(≡C–D)	⊥
2019	ν(C≡C)$_{CCH}$	⊥
1897	ν(C≡C)$_{CCD}$	⊥
~1050	ν(Si–O–Si)$_{TO}$	not ⊥

[a]The symbols ν and δ signify stretching and bending motions, respectively, with subscripts a and s indicating whether the mode is asymmetric or symmetric, respectively. The subscript "TO" indicates a transverse optical Si–O–Si motion. The subscript "sat" indicates a C–H stretching signal arising from unidentified saturated hydrocarbons. The subscripts "CCH" and "CCD" indicate C≡C stretching peaks arising from –CCH and –CCD groups, respectively. The assignments marked with ∗ are tentative. [c]The orientation of the vibrational mode with respect to the plane of the sample surface determined by TIRS is given.

To further demonstrate the reactivity of the lithiated surface, surface-bound Si–C≡C–Li groups were also reacted with neat 4-fluorobenzyl chloride. For comparison, the same reaction was also performed on CH_3–Si(111) surfaces and propynyl-terminated Si(111) (CH_3CC–Si(111)) surfaces (see Chapter 3). Figure 2.16 shows the F 1s XP spectra for CH_3–Si(111), HCC–Si(111), CH_3CC–Si(111), and SiO_x surfaces after sequential reaction with *t*-BuLi followed by 4-fluorobenzyl chloride. HCC–Si(111) surfaces exhibited a F 1s signal at 687.8 eV after reaction with *t*-BuLi followed by 4-fluorobenzyl chloride. XPS was used to provide a rough estimate of the surface coverage of fluorobenzyl groups by use of eq 2.2[55] to yield $\Phi_{\text{fluorobenzyl}} = 0.08 \pm 0.03$ ML, and no residual Cl was observed in the Cl 2s region. The absence of Cl indicated that the 4-fluorobenzyl groups were covalently attached to the surface by nucleophilic substitution, and the LiCl product was removed from the surface. Control experiments showed the absence of detectable F by XPS on CH_3–Si(111) and CH_3CC–Si(111) surfaces that had been reacted sequentially with *t*-BuLi and 4-fluorobenzyl chloride. However, wafers that had been oxidized with a piranha solution and then treated with *t*-BuLi followed by 4-fluorobenzyl chloride produced a F 1s signal centered at 687.0 eV with $\Phi_{\text{fluorobenzyl}} = 0.09$ ML of 4-fluorobenzyl groups bound to the surface. Thus, the 4-fluorobenzyl groups were likely attached at both Si–CCLi and Si–OLi surface sites.

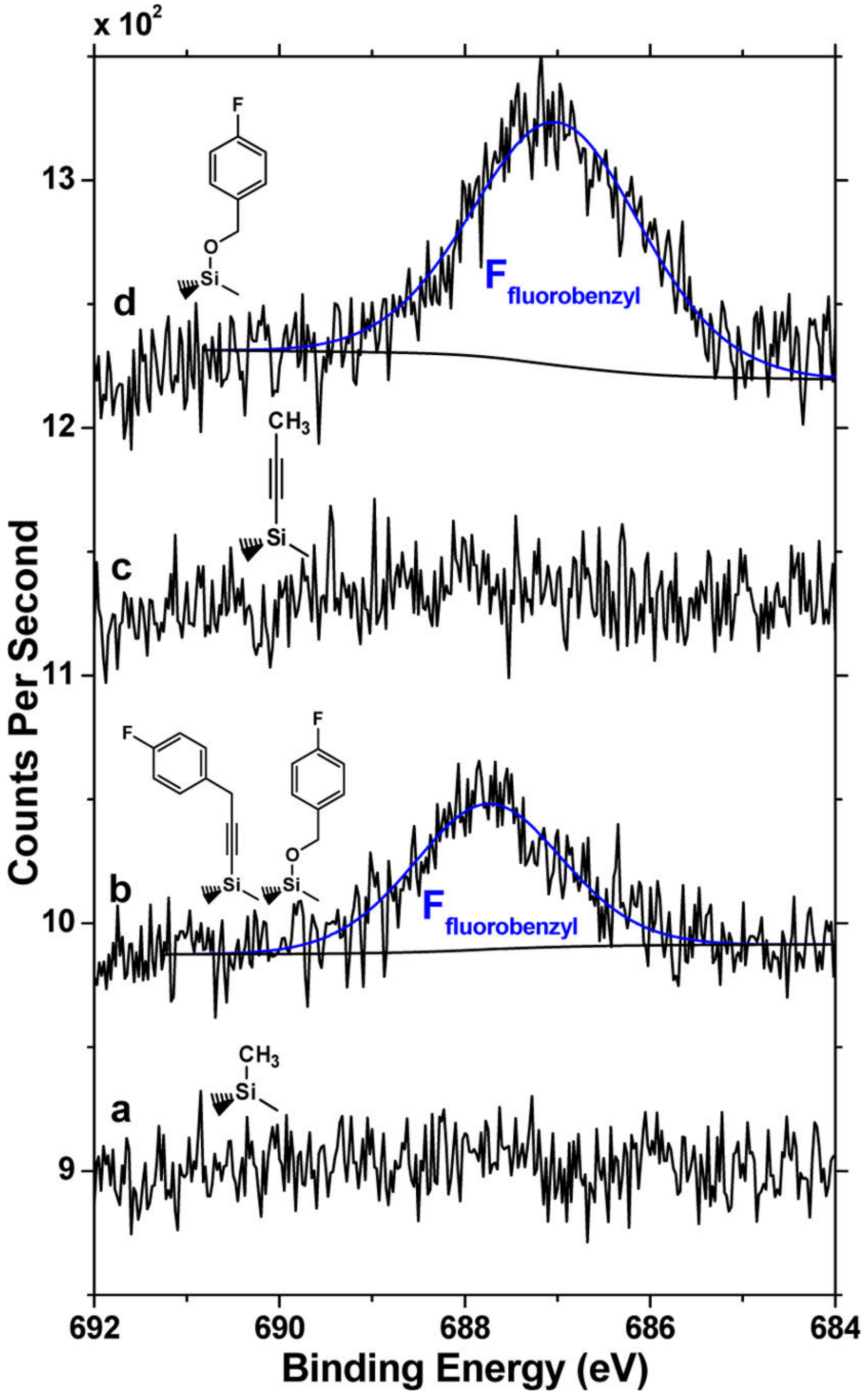

Figure 2.16. High-resolution F 1s XP spectra of (a) CH_3–Si(111), (b) HCC–Si(111), (c) CH_3CC–Si(111), and (d) SiO_x surfaces after reaction with *t*-BuLi followed by 4-fluorobenzyl chloride. Only HCC–Si(111) and SiO_x surfaces showed the presence of detectable F at 687.8 and 687.0 eV, respectively. The proposed structure of the resulting surface is depicted above each spectrum.

2.4 DISCUSSION

2.4.1 Vibrational Spectroscopy of HCC–Si(111) Surfaces

TIRS (Figure 2.1) and HREELS (Figure 2.4) of HCC–Si(111) surfaces prepared using DMSO showed the presence of ≡C–H, C≡C, and Si–C stretching vibrations, providing strong support for the attachment of ethynyl groups perpendicular to the Si(111) surface. Theoretical calculations have predicted the appearance of a ≡C–H stretching mode in the range of 3410 cm^{-1}, with a C≡C stretching mode expected at ~2075 cm^{-1}.[65] The calculations were performed using uncorrected theoretical harmonic frequencies, however, which tend to yield predicted signals that are higher in energy than experimental results for high-frequency modes. Thus, the experimentally observed modes are in agreement with the theoretical calculations for the HCC–Si(111) surface. The presence of a peak at 648 cm^{-1} in the HREEL spectrum is in close agreement with the theoretical prediction of a Si–C stretching signal at approximately 645 cm^{-1},[65] indicating that the ethynyl groups are covalently bound to the Si(111) surface. Theoretical calculations also predict the presence of a ≡C–H bending signal between 568 and 579 cm^{-1}, in addition to a signal between 484 and 492 cm^{-1} resulting from bending of the Si–C≡C–H unit coupled with phonons in the crystal.[65] A small peak in the HREEL spectrum at 477 cm^{-1} and a shoulder on the elastic peak at 346 cm^{-1} could possibly result from the ≡C–H bending and phonon-coupling vibrations, respectively, but may also arise from Si–O bending or other phonon-coupling modes. However, the limited coverage of the Si(111) surface with ethynyl groups hinders the clear detection of these vibrations by current surface-sensitive vibrational spectroscopy techniques.

TIR spectra (Figure 2.1) exhibited peaks ascribable to Si–OH vibrational modes, with the Si–O bond oriented perpendicular to the surface.[57-60, 66] The O–H stretching signal exhibited a reduced intensity at 30° incidence, suggesting that the transition was polarized perpendicular to the surface. However, the proposed geometry of a surface-bound Si–O–H group would be expected to have a significant component of the O–H stretch oriented parallel to the surface. One possible explanation for this could involve hydrogen bonding of the hydroxyl groups to adsorbed water, which could affect the orientation of the O–H bond with respect to the surface. Variation of the amount of adsorbed water may have resulted in the observed reduction in the intensity of the O–H stretching peak at 30° incidence. These vibrational signatures are indicative of HO–Si(111) surface sites, indicating that the HCC–Si(111) surfaces are mixed-composition surfaces in which a fraction of the surface sites are alkylated and a fraction are hydroxylated. Few routes are known to the hydroxylation of crystalline Si surfaces without insertion of O into the Si lattice,[59] and this method has been shown to terminate an estimated 35% of the surface Si(111) sites with –OH groups. The formation of –OH groups on Si surfaces with minimal formation of high-order SiO_x allows for chemical reactions to be performed using versatile hydroxyl group chemistry without introduction of an insulating oxide barrier that is usually intrinsic to oxidized semiconductor surfaces.

The DMSO solvent clearly plays an important role in the formation of Si–OH sites concomitant with Si–CCH sites. Though the DMSO was purchased anhydrous and was dried over molecular sieves prior to use, complete removal of water from DMSO is known to be very difficult, and the surficial –OH groups thus likely arise from trace water in the solvent. The addition of NaCCH to DMSO with trace water will result in deprotonation of the water to yield NaOH, which can undergo nucleophilic reaction with halogenated surface sites. Reaction of NaCCH with Br–Si(111) surfaces with DMA as the solvent also resulted in the observation of ≡C–H and C≡C stretching vibrational signals, though significant SiO_x and hydrocarbon impurities were also present (Figure 2.2). Thus, the solvent controlled the type of surface oxidation that occurred, and surfaces prepared using DMSO were the most well-defined chemically.

2.4.2 Surface Ordering, Stability, and Defects of HCC–Si(111) Surfaces

Although AFM data showed broad atomic terraces functionalized with uniform overlayers, and LEED patterns were consistent with a (1 × 1) surface unit cell, room temperature EC-STM images of HCC–Si(111) surfaces showed that these surfaces did not exhibit the same long-range ordering characteristic of CH_3–Si(111) surfaces. Instead, HCC–Si(111) surfaces showed localized regions of ordering and exhibited small variations in height that were not consistent with the height of a Si(111) step edge. Assuming that the bright regions in Figure 2.9 indicate areas functionalized with –CCH groups, while the dark regions are areas functionalized with –OH groups yielded an estimated coverage of ~0.6 ML –CCH and ~0.4 ML –OH, in good agreement with the surface coverage estimates obtained using XPS. The small difference in height observed between regions was indicative of a difference in the density of states, which could result from a difference in orientation of the –CCH or –OH groups on the surface. The height difference on the same terrace was small (<0.1 nm), and the surfaces exhibited localized regions in which ordering was evident, but significant long-range ordering was not observed for the HCC–Si(111) surface. Given the irreversible nature of the Si–C bond, and the resulting lack of surface mobility of the attached organic groups, steric considerations may in general preclude facile formation of a fully ordered alkylated monolayer over large areas, and the ordering observed for methyl-terminated Si(111) and Ge(111) surfaces[67] are thus remarkable in this respect.

S measurements of HCC–Si(111) (Figure 2.11) surfaces as a function of time exposed to air suggest that this surface is not well-passivated and exhibited behavior similar to H–Si(111) surfaces. The proposed surface structure contains a partial coverage of –OH groups, and the binding of O to oxide-free Si surfaces generally results in the formation of surface trap states that contribute to the degradation of the electronic properties of the surface. While the trap-state density of HCC–Si(111) surfaces was high compared with CH_3–Si(111) surfaces, the trap-state density was well below the detection limit of most surface-sensitive spectroscopies. The high trap-state density for HCC–Si(111) surfaces most likely resulted from oxidation of the surface, which was already partially oxidized as Si–OH and not well protected at Si–C sites by partial coverage with –CCH groups.

The HCC–Si(111) surface exhibited a lower thermal stability than CH_3–Si(111) surfaces, which are known to be stable up to 450 °C in vacuum.[28, 31] The ethynyl groups underwent saturation as they reacted with adventitious C species on the sample or in the vacuum chamber, and annealing from 600–700 °C resulted in larger amounts of C on the sample surface. HCC–Si(111) surfaces showed the largest intensity SiC peak upon annealing to 700 °C, and an overall increase in C 1s peak area was observed, suggesting hydrocarbons in the atmosphere reacted with and were bound to the surface upon heating above 500 °C. These results suggest that the −CCH groups readily undergo reaction with other species adsorbed on the surface and in the vacuum chamber. The results indicate that the chemical reactivity of the surface is increased for HCC–Si(111) surfaces compared with CH_3–Si(111) surfaces.

2.4.3 Reactivity of HCC–Si(111) Surfaces

Terminal alkynes can be deprotonated readily by reaction with a strong base, such as *t*-BuLi. Consistently, HCC–Si(111) surfaces were shown to undergo reaction with *t*-BuLi to form a surface-bound lithium acetylide. Many surface functionalization techniques rely on nucleophilic attack of the surface by a molecular species, whereas generation of a surface-bound nucleophile expands the surface chemistry toolkit for functionalization of Si surfaces. The presence of the surface-bound organolithium was demonstrated by reaction with CD_3OD to yield deuterated ethynyl groups on the surface. TIRS (Figure 2.12) showed the appearance of a pair of $\nu(\equiv C{-}D)$ peaks along with a $(C\equiv C)_{CCD}$ peak. The difference between the $\nu(\equiv C{-}H)$ and $\nu(\equiv C{-}D)$ peak positions was ~730 cm^{-1}, which is consistent with previous work that has shown the difference in peak position from C–H to C–D stretching to be ~750 cm^{-1} on C_2H_5–Si(111) surfaces.[24] The shift from $(C\equiv C)_{CCH}$ to $(C\equiv C)_{CCD}$ was considerably smaller (122 cm^{-1}) because the D atom interacts indirectly with the C≡C stretching mode.

Attachment of 4-fluorobenzyl groups to the surface of HCC–Si(111) surfaces functionalized 8 ± 3% of surface sites with 4-fluorobenzyl groups (Figure 2.16). The absence of Cl observed in Cl 2s spectra suggests that the 4-fluorobenzyl groups were bound to the surface by nucleophilic substitution. Additionally, since no F 1s signal was observed for CH_3–Si(111) and CH_3CC–Si(111) surfaces subjected to the same treatment, the HCC–Si(111) surface appears to possess unique chemistry that allows for the generation of surface-bound nucleophiles. However, SiO_x samples subjected to deprotonation in *t*-BuLi and reaction with 4-fluorobenzyl chloride similarly yielded a surface with ~9% of a ML of 4-fluorobenzyl groups, indicating that surface-bound –OLi groups can also react with 4-fluorobenzyl chloride in a nucleophilic substitution reaction. Thus, deprotonation of HCC–Si(111) surfaces to yield both –CCLi and –OLi groups on the surface allowed both nucleophile species to react with the 4-fluorobenzyl chloride electrophile.

2.4.4 Comparison with Previously Reported Syntheses and Surface Spectroscopy

The synthesis of HCC–Si(111) surfaces has been reported previously, albeit with minimal spectroscopic characterization of the resulting surfaces.[44-48] Table 2.4 summarizes the synthetic methods, surface characterization techniques employed, and results of the prior studies. For putative HCC–Si(111) surfaces prepared from Cl–Si(111) surfaces reacted with NaCCH in THF,[44] the position of the C≡C stretch was reported as 2179 cm^{-1},[44] which is 160 cm^{-1} higher than the signal observed in this work (2019 cm^{-1}) and ~100 cm^{-1} higher than the upper estimate predicted by theoretical calculations (2075 cm^{-1}).[65] We attempted to reproduce the results of those reports, but our attempts were unsuccessful except in certain respects on unpredictable occasions. Anodic deposition of HCCMgCl and HCCMgBr on H–Si(111) surfaces has also been reported for the preparation of HCC–Si(111) and yields a C≡C stretch at ~2040 cm^{-1}.[46-47] The C≡C stretch at 2019 cm^{-1} observed herein agrees more closely with the behavior of surfaces prepared by anodic deposition, and is in better agreement with theoretical calculations than the signal reported at 2179 cm^{-1}.[65] HCC–Si(111) surfaces prepared from the reaction of Cl–Si(111) surfaces with NaCCH in xylenes reported no observable C≡C stretch.[45] Observation of ethynyl ≡C−H stretching at ~3300 cm^{-1} has been reported for samples prepared by anodic deposition that yielded a polymeric layer[47] as well as for samples prepared by reaction of H/D–Si(111) surfaces with HCCMgBr in THF.[48] The presence of a Si–C stretching peak at 660 cm^{-1} has only been previously observed for samples prepared by reaction of HCCMgBr with H/D–Si(111) surfaces, which showed incomplete reactivity and contamination from saturated hydrocarbons.[48] The observation of ethynyl ≡C−H stretching signals at 3307 and 3296 cm^{-1}, in addition to the C≡C stretch at 2019 cm^{-1} and Si–C stretch at 648 cm^{-1}, provides strong evidence for the formation of HCC–Si(111) surfaces using the reaction chemistry described herein.

Table 2.4. Summary of Prior Reports of Synthesis and Characterization of Ethynyl-Terminated Si Surfaces

Publication	Reaction Conditions	Characterization and Evidence for Structure
ref[44]	Cl–Si(111) reacted with NaCCH in THF to give Si–CCH surfaces, respectively.	XPS: C 1s XP peak at 284.0 eV used to suggest C bound to Si. Coverage estimated to be 0.9 ± 0.1 ML for Si–CCH relative to Si–CH_3. No evidence for SiO_x in Si 2p. IR: Si–CCH exhibits C≡C stretch at 2179 cm^{-1} polarized perpendicular to the surface. Electrochemical measurements show no Si–H oxidation peak in aqueous electrolyte. Si–CCH surfaces were reacted with *n*-BuLi, then 4-bromobenzotrifluoride to show C bound to F by XPS.
ref[45]	Cl–Si(111) reacted with NaCCH in xylenes/mineral oil at 130 °C for 5 h to give Si–CCH surfaces.	XPS: C 1s XP peak at 283.8 eV used to suggest C bound to Si. Coverage with –CCH groups estimated to be 0.97 ± 0.05 ML relative to Si–CH_3. Si 2p showed minimal oxidation after preparation, with 0.25 ML of SiO_x present after 6 days in air. IR: Disappearance of Si–H stretching after functionalization was used to show complete termination. Contact-angle measurements with water were 77 ± 2° for the Si–CCH surface. Click chemistry was performed via Cu(I)-catalyzed reaction of Si–CCH surfaces with an azide-functionalized benzoquinone. The surface coverage was estimated to be ~0.07 ML of benzoquinone, which was then removed and ferrocene was attached with a coverage of 0.005 ML.
ref[46]	Anodic grafting of HCCMgBr in THF to H–Si(111) surfaces. Current density was 100 µA cm^{-2} with a pulse length of 0.1 s for 100 pulses.	IR: The reaction was monitored by IR. As anodic pulses were applied, the Si–H stretching peak at ~2080 cm^{-1} was lost and the C≡C stretch at ~2040 cm^{-1} peak grew in, though quantitative analysis was precluded by significant overlap of the two signals. The position of the C≡C stretch is in best agreement with the results reported in this work.
ref[47]	Anodic grafting of HCCMgCl or HCCMgBr in THF to H–Si(111) surfaces. The current density was 0.5 or 0.02 mA cm^{-2} applied over 15–20 min.	SEM indicated the presence of a polymeric layer for all samples prepared. IR: All samples showed disappearance of Si–H after anodic deposition. Samples prepared from HCCMgCl showed acetylenic ≡C–H stretching at ~3300 cm^{-1} as well as C≡C stretching at ~2046 cm^{-1}. Also present were modes ascribed to the presence of saturated alkyl chains, indicating that the C≡C bond became saturated during grafting and polymerization. Residual Cl was observed on the surface, and the authors postulate it was inserted into the polymer. SXPS: A C 1s XP peak at 283.7 eV was used to qualitatively suggest C bound to Si. Si 2p XP spectra showed shift in surface Si to higher binding energy, further suggesting that the surface Si is bound to C. The observed polymer layer is inconsistent with results reported by Teyssot et al., who concluded the HCCMgBr does not polymerize on H-Si(111) surfaces upon application of anodic current.
ref[48]	H–Si(111) and D–Si(111) reacted with HCCMgBr in THF at 60–65 °C for 4.25–5 h to yield HCC–Si(111) surfaces	Multiple internal infrared reflection absorption spectroscopy (MI-IRAS) and HREELS used to show vibrational structure. Ethynyl ≡C−H stretch observed at ~3300 cm^{-1} and C≡C stretch observed at 2020 cm^{-1}, in agreement with the results reported in this work. A peak at 660 cm^{-1} was attributed to Si–C stretching. A significant fraction of Si–H and Si–D surface sites remained unreacted. Surfaces were contaminated with saturated hydrocarbons and a small amount of SiO_x was observed.

2.5 CONCLUSIONS

HCC–Si(111) surfaces have been synthesized and characterized by a variety of spectroscopic methods. TIRS and HREELS data show the characteristic vibrational modes for Si–C≡C–H groups covalently bound perpendicular to the surface. HCC–Si(111) surfaces also exhibited the presence of Si–OH vibrational modes when prepared in DMSO. XPS of HCC–Si(111) surfaces exhibited $\Phi_{\text{Si–CCH}} = 0.63 \pm 0.08$ ML and $\Phi_{\text{Si–OH}} = 0.35 \pm 0.03$ ML. The prepared surfaces exhibited no detectable unreacted Si–H or Si–Br sites. Annealing of HCC–Si(111) surfaces in vacuum resulted in the appearance of different C species at elevated temperature, including SiC that formed on the surface. AFM and LEED data showed that the surfaces exhibited terraced structures and ordering comparable to that of CH_3–Si(111) surfaces, though EC-STM data showed that the surfaces did not exhibit the long-range ordering of CH_3–Si(111) surfaces. HCC–Si(111) surfaces were deprotonated using *t*-BuLi to form a surface-bound lithium acetylide, which was shown to undergo a reaction with electrophiles.

The complete vibrational spectra for the HCC−Si(111) surfaces presented in this work definitively establish the covalent attachment of ethynyl and propynyl groups to the Si(111) surface. Vibrational spectroscopy, which is perhaps the most powerful tool for surface structural analysis, used in tandem with XPS, LEED, AFM, EC-STM, and *S* measurements provide a clear picture of the surface structure, allowing for the development of structure-function relationships, new chemistries, and, by extension, new technologies.

2.6 REFERENCES

1. Bansal, A.; Lewis, N. S. Stabilization of Si Photoanodes in Aqueous Electrolytes through Surface Alkylation. *J. Phys. Chem. B* **1998**, *102*, 4058-4060.
2. Bansal, A.; Lewis, N. S. Electrochemical Properties of (111)-Oriented n-Si Surfaces Derivatized with Covalently-Attached Alkyl Chains. *J. Phys. Chem. B* **1998**, *102*, 1067-1070.
3. Webb, L. J.; Lewis, N. S. Comparison of the Electrical Properties and Chemical Stability of Crystalline Silicon(111) Surfaces Alkylated Using Grignard Reagents or Olefins with Lewis Acid Catalysts. *J. Phys. Chem. B* **2003**, *107*, 5404-5412.
4. Royea, W. J.; Juang, A.; Lewis, N. S. Preparation of Air-Stable, Low Recombination Velocity Si(111) Surfaces through Alkyl Termination. *Appl. Phys. Lett.* **2000**, *77*, 1988-1990.
5. Yablonovitch, E.; Allara, D. L.; Chang, C. C.; Gmitter, T.; Bright, T. B. Unusually Low Surface-Recombination Velocity on Silicon and Germanium Surfaces. *Phys. Rev. Lett.* **1986**, *57*, 249-252.
6. Johansson, E.; Boettcher, S. W.; O'Leary, L. E.; Poletayev, A. D.; Maldonado, S.; Brunschwig, B. S.; Lewis, N. S. Control of the pH-Dependence of the Band Edges of Si(111) Surfaces Using Mixed Methyl/Allyl Monolayers. *J. Phys. Chem. C* **2011**, *115*, 8594-8601.
7. Li, Y.; O'Leary, L. E.; Lewis, N. S.; Galli, G. Combined Theoretical and Experimental Study of Band-Edge Control of Si through Surface Functionalization. *J. Phys. Chem. C* **2013**, *117*, 5188-5194.

8. Wong, K. T.; Lewis, N. S. What a Difference a Bond Makes: The Structural, Chemical, and Physical Properties of Methyl-Terminated Si(111) Surfaces. *Acc. Chem. Res.* **2014**, *47*, 3037-3044.
9. Walter, M. G.; Warren, E. L.; McKone, J. R.; Boettcher, S. W.; Mi, Q.; Santori, E. A.; Lewis, N. S. Solar Water Splitting Cells. *Chem. Rev.* **2010**, *110*, 6446-6473.
10. Neergaard Waltenburg, H.; Yates, J. T. Surface Chemistry of Silicon. *Chem. Rev.* **1995**, *95*, 1589-1673.
11. Shen, X.; Sun, B.; Yan, F.; Zhao, J.; Zhang, F.; Wang, S.; Zhu, X.; Lee, S. High-Performance Photoelectrochemical Cells from Ionic Liquid Electrolyte in Methyl-Terminated Silicon Nanowire Arrays. *ACS Nano* **2010**, *4*, 5869-5876.
12. Zhang, F.; Liu, D.; Zhang, Y.; Wei, H.; Song, T.; Sun, B. Methyl/Allyl Monolayer on Silicon: Efficient Surface Passivation for Silicon-Conjugated Polymer Hybrid Solar Cell. *ACS Appl. Mater. Inter.* **2013**, *5*, 4678-4684.
13. Hu, S.; Shaner, M. R.; Beardslee, J. A.; Lichterman, M.; Brunschwig, B. S.; Lewis, N. S. Amorphous TiO_2 coatings stabilize Si, GaAs, and GaP photoanodes for efficient water oxidation. *Science* **2014**, *344*, 1005-1009.
14. Guisinger, N. P.; Greene, M. E.; Basu, R.; Baluch, A. S.; Hersam, M. C. Room Temperature Negative Differential Resistance through Individual Organic Molecules on Silicon Surfaces. *Nano Lett.* **2004**, *4*, 55-59.
15. Yates, J. T. A New Opportunity in Silicon-Based Microelectronics. *Science* **1998**, *279*, 335-336.

16. Haick, H.; Hurley, P. T.; Hochbaum, A. I.; Yang, P.; Lewis, N. S. Electrical Characteristics and Chemical Stability of Non-Oxidized, Methyl-Terminated Silicon Nanowires. *J. Am. Chem. Soc.* **2006**, *128*, 8990-8991.
17. O'Leary, L. E.; Strandwitz, N. C.; Roske, C. W.; Pyo, S.; Brunschwig, B. S.; Lewis, N. S. Use of Mixed CH_3–/$HC(O)CH_2CH_2$–Si(111) Functionality to Control Interfacial Chemical and Electronic Properties During the Atomic-Layer Deposition of Ultrathin Oxides on Si(111). *J. Phys. Chem. Lett.* **2015**, *6*, 722-726.
18. Maldonado, S.; Knapp, D.; Lewis, N. S. Near-Ideal Photodiodes from Sintered Gold Nanoparticle Films on Methyl-Terminated Si(111) Surfaces. *J. Am. Chem. Soc.* **2008**, *130*, 3300-3301.
19. Lattimer, J. R. C.; Blakemore, J. D.; Sattler, W.; Gul, S.; Chatterjee, R.; Yachandra, V. K.; Yano, J.; Brunschwig, B. S.; Lewis, N. S.; Gray, H. B. Assembly, Characterization, and Electrochemical Properties of Immobilized Metal Bipyridyl Complexes on Silicon(111) Surfaces. *Dalton Trans.* **2014**, *43*, 15004-15012.
20. Lattimer, J. R. C.; Brunschwig, B. S.; Lewis, N. S.; Gray, H. B. Redox Properties of Mixed Methyl/Vinylferrocenyl Monolayers on Si(111) Surfaces. *J. Phys. Chem. C* **2013**, *117*, 27012-27022.
21. O'Leary, L. E.; Johansson, E.; Brunschwig, B. S.; Lewis, N. S. Synthesis and Characterization of Mixed Methyl/Allyl Monolayers on Si(111). *J. Phys. Chem. B* **2010**, *114*, 14298-14302.
22. O'Leary, L. E.; Rose, M. J.; Ding, T. X.; Johansson, E.; Brunschwig, B. S.; Lewis, N. S. Heck Coupling of Olefins to Mixed Methyl/Thienyl Monolayers on Si(111) Surfaces. *J. Am. Chem. Soc.* **2013**, *135*, 10081-10090.

23. Webb, L. J.; Rivillon, S.; Michalak, D. J.; Chabal, Y. J.; Lewis, N. S. Transmission Infrared Spectroscopy of Methyl- and Ethyl-Terminated Silicon(111) Surfaces. *J. Phys. Chem. B* **2006**, *110*, 7349-7356.
24. Johansson, E.; Hurley, P. T.; Brunschwig, B. S.; Lewis, N. S. Infrared Vibrational Spectroscopy of Isotopically Labeled Ethyl-Terminated Si(111) Surfaces Prepared Using a Two-Step Chlorination/Alkylation Procedure. *J. Phys. Chem. C* **2009**, *113*, 15239-15245.
25. Rivillon, S.; Chabal, Y. J. Alkylation of Silicon(111) Surfaces. *J. Phys. IV* **2006**, *132*, 195-198.
26. Rivillon Amy, S.; Michalak, D. J.; Chabal, Y. J.; Wielunski, L.; Hurley, P. T.; Lewis, N. S. Investigation of the Reactions during Alkylation of Chlorine-Terminated Silicon (111) Surfaces. *J. Phys. Chem. C* **2007**, *111*, 13053-13061.
27. Yamada, T.; Kawai, M.; Wawro, A.; Suto, S.; Kasuya, A. HREELS, STM, and STS study of CH_3-Terminated Si(111)-(1 x 1) Surface. *J. Chem. Phys.* **2004**, *121*, 10660-10667.
28. Hunger, R.; Fritsche, R.; Jaeckel, B.; Jaegermann, W.; Webb, L. J.; Lewis, N. S. Chemical and Electronic Characterization of Methyl-Terminated Si(111) Surfaces by High-Resolution Synchrotron Photoelectron Spectroscopy. *Phys. Rev. B* **2005**, *72*, 045317.
29. Webb, L. J.; Michalak, D. J.; Biteen, J. S.; Brunschwig, B. S.; Chan, A. S. Y.; Knapp, D. W.; Meyer, H. M.; Nemanick, E. J.; Traub, M. C.; Lewis, N. S. High-Resolution Soft X-ray Photoelectron Spectroscopic Studies and Scanning Auger Microscopy

Studies of the Air Oxidation of Alkylated Silicon(111) Surfaces. *J. Phys. Chem. B* **2006**, *110*, 23450-23459.

30. Webb, L. J.; Nemanick, E. J.; Biteen, J. S.; Knapp, D. W.; Michalak, D. J.; Traub, M. C.; Chan, A. S. Y.; Brunschwig, B. S.; Lewis, N. S. High-Resolution X-ray Photoelectron Spectroscopic Studies of Alkylated Silicon(111) Surfaces. *J. Phys. Chem. B* **2005**, *109*, 3930-3937.
31. Jaeckel, B.; Hunger, R.; Webb, L. J.; Jaegermann, W.; Lewis, N. S. High-Resolution Synchrotron Photoemission Studies of the Electronic Structure and Thermal Stability of CH_3- and C_2H_5-Functionalized Si(111) Surfaces. *J. Phys. Chem. C* **2007**, *111*, 18204-18213.
32. Becker, J. S.; Brown, R. D.; Johansson, E.; Lewis, N. S.; Sibener, S. J. Helium Atom Diffraction Measurements of the Surface Structure and Vibrational Dynamics of CH_3--Si(111) and CD_3--Si(111) Surfaces. *J. Chem. Phys.* **2010**, *133*, 104705.
33. Brown, R. D.; Hund, Z. M.; Campi, D.; O'Leary, L. E.; Lewis, N. S.; Bernasconi, M.; Benedek, G.; Sibener, S. J. Hybridization of Surface Waves with Organic Adlayer Librations: A Helium Atom Scattering and Density Functional Perturbation Theory Study of Methyl-Si(111). *Phys. Rev. Lett.* **2013**, *110*, 156102.
34. Brown, R. D.; Hund, Z. M.; Campi, D.; O'Leary, L. E.; Lewis, N. S.; Bernasconi, M.; Benedek, G.; Sibener, S. J. The Interaction of Organic Adsorbate Vibrations with Substrate Lattice Waves in Methyl-Si(111)-(1 × 1). *J. Chem. Phys.* **2014**, *141*, 024702.
35. Malyk, S.; Shalhout, F. Y.; O'Leary, L. E.; Lewis, N. S.; Benderskii, A. V. Vibrational Sum Frequency Spectroscopic Investigation of the Azimuthal Anisotropy and

Rotational Dynamics of Methyl-Terminated Silicon(111) Surfaces. *J. Phys. Chem. C* **2012**, *117*, 935-944.

36. Yu, H.; Webb, L. J.; Ries, R. S.; Solares, S. D.; Goddard, W. A.; Heath, J. R.; Lewis, N. S. Low-Temperature STM Images of Methyl-Terminated Si(111) Surfaces. *J. Phys. Chem. B* **2004**, *109*, 671-674.
37. Nemanick, E. J.; Solares, S. D.; Goddard, W. A.; Lewis, N. S. Quantum Mechanics Calculations of the Thermodynamically Controlled Coverage and Structure of Alkyl Monolayers on Si(111) Surfaces. *J. Phys. Chem. B* **2006**, *110*, 14842-14848.
38. Nemanick, E. J.; Hurley, P. T.; Brunschwig, B. S.; Lewis, N. S. Chemical and Electrical Passivation of Silicon (111) Surfaces through Functionalization with Sterically Hindered Alkyl Groups. *J. Phys. Chem. B* **2006**, *110*, 14800-14808.
39. Plass, K. E.; Liu, X.; Brunschwig, B. S.; Lewis, N. S. Passivation and Secondary Functionalization of Allyl-Terminated Si(111) Surfaces. *Chem. Mater.* **2008**, *20*, 2228-2233.
40. Miller, T.; Teplyakov, A. V. Attachment Chemistry of PCBM to a Primary-Amine-Terminated Organic Monolayer on a Si(111) Surface. *Langmuir* **2014**, *30*, 5105-5114.
41. Li, M.; Dai, M.; Chabal, Y. J. Atomic Layer Deposition of Aluminum Oxide on Carboxylic Acid-Terminated Self-Assembled Monolayers. *Langmuir* **2009**, *25*, 1911-1914.
42. Strother, T.; Hamers, R. J.; Smith, L. M. Covalent Attachment of Oligodeoxyribonucleotides to Amine-Modified Si (001) Surfaces. *Nucleic Acids Res.* **2000**, *28*, 3535-3541.

43. Strother, T.; Cai, W.; Zhao, X.; Hamers, R. J.; Smith, L. M. Synthesis and Characterization of DNA-Modified Silicon (111) Surfaces. *J. Am. Chem. Soc.* **2000**, *122*, 1205-1209.
44. Hurley, P. T.; Nemanick, E. J.; Brunschwig, B. S.; Lewis, N. S. Covalent Attachment of Acetylene and Methylacetylene Functionality to Si(111) Surfaces: Scaffolds for Organic Surface Functionalization while Retaining Si−C Passivation of Si(111) Surface Sites. *J. Am. Chem. Soc.* **2006**, *128*, 9990-9991.
45. Rohde, R. D.; Agnew, H. D.; Yeo, W.-S.; Bailey, R. C.; Heath, J. R. A Non-Oxidative Approach toward Chemically and Electrochemically Functionalizing Si(111). *J. Am. Chem. Soc.* **2006**, *128*, 9518-9525.
46. Teyssot, A.; Fidélis, A.; Fellah, S.; Ozanam, F.; Chazalviel, J. N. Anodic Grafting of Organic Groups on the Silicon Surface. *Electrochim. Acta* **2002**, *47*, 2565-2571.
47. Yang, F.; Hunger, R.; Roodenko, K.; Hinrichs, K.; Rademann, K.; Rappich, J. Vibrational and Electronic Characterization of Ethynyl Derivatives Grafted onto Hydrogenated Si(111) Surfaces. *Langmuir* **2009**, *25*, 9313-9318.
48. Yamada, T.; Shirasaka, K.; Noto, M.; Kato, H. S.; Kawai, M. Adsorption of Unsaturated Hydrocarbon Moieties on H:Si(111) by Grignard Reaction. *J. Phys. Chem. B* **2006**, *110*, 7357-7366.
49. Gleason-Rohrer, D. C.; Brunschwig, B. S.; Lewis, N. S. Measurement of the Band Bending and Surface Dipole at Chemically Functionalized Si(111)/Vacuum Interfaces. *J. Phys. Chem. C* **2013**, *117*, 18031-18042.

50. Rivillon, S.; Chabal, Y. J.; Webb, L. J.; Michalak, D. J.; Lewis, N. S.; Halls, M. D.; Raghavachari, K. Chlorination of Hydrogen-Terminated Silicon (111) Surfaces. *J. Vac. Sci. Technol. A* **2005**, *23*, 1100-1106.
51. Briggs, D.; Seah, M. P. *Practical Surface Analysis: Auger and X-ray Photoelectron Spectroscopy*, 2nd ed.; John Wiley & Sons, Inc.: New York, 1990; Vol. 1.
52. Haber, J. A.; Lewis, N. S. Infrared and X-ray Photoelectron Spectroscopic Studies of the Reactions of Hydrogen-Terminated Crystalline Si(111) and Si(100) Surfaces with Br_2, I_2, and Ferrocenium in Alcohol Solvents. *J. Phys. Chem. B* **2002**, *106*, 3639-3656.
53. van der Marel, C.; Yildirim, M.; Stapert, H. R. Multilayer Approach to the Quantitative Analysis of X-ray Photoelectron Spectroscopy Results: Applications to Ultrathin SiO_2 on Si and to Self-Assembled Monolayers on Gold. *J. Vac. Sci. Technol. A* **2005**, *23*, 1456-1470.
54. Seah, M. P.; Spencer, S. J. Ultrathin SiO_2 on Si II. Issues in Quantification of the Oxide Thickness. *Surf. Interface Anal.* **2002**, *33*, 640-652.
55. Brown, E. S.; Peczonczyk, S. L.; Maldonado, S. Wet Chemical Functionalization of GaP(111)B through a Williamson Ether-Type Reaction. *J. Phys. Chem. C* **2015**, *119*, 1338-1345.
56. Asami, K.; Hashimoto, K.; Shimodaira, S. XPS Determination of Compositions of Alloy Surfaces and Surface Oxides on Mechanically Polished Iron-Chromium Alloys. *Corros. Sci.* **1977**, *17*, 713-723.
57. Weldon, M. K.; Stefanov, B. B.; Raghavachari, K.; Chabal, Y. J. Initial H_2O-Induced Oxidation of Si(100)-(2 x 1). *Phys. Rev. Lett.* **1997**, *79*, 2851-2854.

58. Struck, L. M.; Eng Jr, J.; Bent, B. E.; Flynn, G. W.; Chabal, Y. J.; Christman, S. B.; Chaban, E. E.; Raghavachari, K.; Williams, G. P.; Radermacher, K.; Mantl, S. Vibrational Study of Silicon Oxidation: H_2O on Si(100). *Surf. Sci.* **1997**, *380*, 444-454.
59. Michalak, D. J.; Amy, S. R.; Aureau, D.; Dai, M.; Esteve, A.; Chabal, Y. J. Nanopatterning Si(111) Surfaces as a Selective Surface-Chemistry Route. *Nat. Mater.* **2010**, *9*, 266-271.
60. Rao, G. R. Infrared Reflection Absorption Study of Water Interaction with H-Terminated Si(100) Surfaces. *Bull. Mater. Sci.* **2004**, *27*, 497-500.
61. Michalak, D. J.; Rivillon, S.; Chabal, Y. J.; Estève, A.; Lewis, N. S. Infrared Spectroscopic Investigation of the Reaction of Hydrogen-Terminated, (111)-Oriented, Silicon Surfaces with Liquid Methanol. *J. Phys. Chem. B* **2006**, *110*, 20426-20434.
62. Contarini, S.; Howlett, S. P.; Rizzo, C.; De Angelis, B. A. XPS Study on the Dispersion of Carbon Additives in Silicon Carbide Powders. *Appl. Surf. Sci.* **1991**, *51*, 177-183.
63. Muehlhoff, L.; Choyke, W. J.; Bozack, M. J.; Yates, J. T. Comparative Electron Spectroscopic Studies of Surface Segregation on SiC(0001) and SiC($000\bar{1}$). *J. Appl. Phys.* **1986**, *60*, 2842-2853.
64. Becker, R. S.; Golovchenko, J. A.; McRae, E. G.; Swartzentruber, B. S. Tunneling Images of Atomic Steps on the Si(111)7x7 Surface. *Phys. Rev. Lett.* **1985**, *55*, 2028-2031.
65. Ferguson, G. A.; Raghavachari, K. Collective Vibrations in Cluster Models for Semiconductor Surfaces: Vibrational Spectra of Acetylenyl and Methylacetylenyl Functionalized Si(111). *J. Chem. Phys.* **2007**, *127*, 194706.

66. Kato, H. S.; Kawai, M.; Akagi, K.; Tsuneyuki, S. Interaction of Condensed Water Molecules with Hydroxyl and Hydrogen Groups on Si(001). *Surf. Sci.* **2005**, *587*, 34-40.

67. Wong, K. T.; Kim, Y.-G.; Soriaga, M. P.; Brunschwig, B. S.; Lewis, N. S. Synthesis and Characterization of Atomically Flat Methyl-Terminated Ge(111) Surfaces. *J. Am. Chem. Soc.* **2015**.